Enhanced mixed interpolation XFEM formulations for discontinuous Timoshenko beam and Mindlin-Reissner plate

M. Toolabi[a*], A. S. Fallah[b], P. M. Baiz[b], L. A. Louca[c]

[a]Department of Mechanical Engineering, City and Guilds Building, South Kensington Campus, Imperial College London, London, SW7 2AZ, UK
[b]Department of Aeronautics, Roderic Hill Building, South Kensington Campus, Imperial College London, London, SW7 2AZ, UK
[c]Department of Civil and Environmental Engineering, Skempton Building, South Kensington Campus, Imperial College London, London, SW7 2AZ, UK

Abstract

Shear locking is a major issue emerging in the computational formulation of beam and plate finite elements of minimal number of degrees-of-freedom as it leads to artificial over-stiffening. In this paper discontinuous Timoshenko beam and Mindlin-Reissner plate elements are developed by adopting the Hellinger-Reissner (HR) functional with the displacements and through-thickness shear strains as degrees-of-freedom. Heterogeneous beams and plates with weak discontinuity are considered and the mixed formulation has been combined with the eXtended Finite Element Method (XFEM) thus mixed enrichment functions are used. Both the displacement and the shear strain fields are enriched as opposed to the traditional XFEM where only the displacement functions are enriched. The enrichment type is restricted to extrinsic mesh-based topological local enrichment. The results from the proposed formulation correlate well with analytical solution in the case of the beam and in the case of the Mindlin-Reissner plate with those of a finite element package (ABAQUS) and classical Finite Element Method (FEM) and show higher rates of convergence. In all cases, the proposed method captures strain discontinuity accurately. Thus, the proposed method provides an accurate and a computationally more efficient way for the formulation of beam and plate finite elements of minimal number of degrees of freedom.

Keywords: Hellinger-Reissner (HR) functional, mixed interpolation of tensorial components (MITC), shear locking, Timoshenko beam, Mindlin-Reissner plate, extended finite element method (XFEM)

* To whom correspondence should be addressed:
Email: milad.toolabi04@imperial.ac.uk

Nomenclature

Latin lower case

d	depth/breadth of the beam $[L]$
$\boldsymbol{f}^B$	body force field $[ML^{-2}T^{-2}]$
$\boldsymbol{f}^{S_f}$	surface force field $[ML^{-1}T^{-2}]$
$\boldsymbol{f}^{S_u}$	reaction force field at the support $[ML^{-1}T^{-2}]$
h	height of the beam $[L]$
q	shear force $[MLT^{-2}]$
t_r	rise time of pressure $[T]$
$\mathbf{u}$	displacement field $[L]$
$\widehat{\boldsymbol{u}}$	nodal degrees-of-freedom $[L]$
$\mathbf{u}^{S_f}$	surface displacement field $[L]$
$\boldsymbol{u}^{S_u}$	prescribed displacement field at the support $[L]$
$\boldsymbol{u}_p$	prescribed displacement field $[L]$
w	vertical displacement $[L]$
w_i	section's vertical displacement $[L]$
x^*	position of the discontinuity $[L]$

Latin upper case

A	section cross sectional area $[L^2]$
A_{w_i}	enriched vertical displacement degrees-of-freedom $[L]$
A_{θ_i}	enriched rotational degrees-of-freedom $[L]$
$A_{\hat{\varepsilon}_i}$	enriched strain degrees-of-freedom [1]
$\boldsymbol{B}_{\boldsymbol{S}}^{\boldsymbol{AS}}$	matrix relating nodal shear strain to the field shear strain [1]
$\mathbf{B_s}$	matrix relating nodal displacement to the field shear strain [1]
$\mathbf{B_b}$	matrix relating nodal displacement to the field strain in x direction [1]
$\mathbf{C}$	matrix of material constant $[ML^{-1}T^{-2}]$
$\boldsymbol{C}_b$	matrix of material constant (bending) $[ML^{-1}T^{-2}]$
$\boldsymbol{C}_s$	matrix of material constant (shear) $[ML^{-1}T^{-2}]$
E_i	section's Young's modulus $[ML^{-1}T^{-2}]$
G_i	section's shear modulus $[ML^{-1}T^{-2}]$
E_i	section's Young's modulus $[ML^{-1}T^{-2}]$
H	Heaviside function [1]
$\boldsymbol{H}$	matrix relating nodal displacement to the field displacement [1]
I	second moment of area $[L^4]$
J	Jacobian $[L]$
L	length of the beam $[L]$
N_i	shape function of node *i* [1]
Q_i	section's shear force $[MLT^{-2}]$
S	surface area $[L^2]$
V	volume $[L^3]$

Greek lower case

$\gamma_{i_{xz}}$	section's shear strain in xz-plane [1]

$\gamma_{i_{yz}}$	section's shear strain in yz-plane [1]
γ_{xz}^{AS}	assumed constant shear strain in xz-plane [1]
γ_{yz}^{AS}	assumed constant shear strain in yz-plane [1]
$\widehat{\boldsymbol{\gamma}}$	nodal shear strain degree-of-freedom [1]
$\boldsymbol{\varepsilon}$	strain field [1]
$\boldsymbol{\varepsilon_b}$	bending strain field [1]
$\boldsymbol{\varepsilon_s}$	shear strain field [1]
ε_{xx}	strain in the x direction [1]
ε_{yy}	strain in the y direction [1]
θ_i	section's rotation [1]
θ_{x_i}	section's rotation around y-axis [1]
θ_{y_i}	section's rotation around x-axis [1]
κ	shear correction factor [1]
$\boldsymbol{\lambda_\varepsilon}$	Lagrange multiplier field corresponding to strain $[ML^{-1}T^{-2}]$
$\boldsymbol{\lambda_u}$	Lagrange multiplier field corresponding to displacement $[ML^{-1}T^{-2}]$
ν	Poisson's ratio [1]
$\boldsymbol{\tau}$	stress field $[ML^{-1}T^{-2}]$
ψ	enrichment function [1]
$\Delta\psi_i$	difference between the node *i* enrichment value and position x $[L]$

Greek upper case

$\emptyset_J$	Level set $[L]$

1. Introduction

Weak discontinuities are encountered in a variety of circumstances; from the necessity of adopting bi-materials as a functionality requirement. For instance, in the case of a thermostat to optimization of performance when two materials of different mechanical behaviour are tied together and from the formation of a layer of oxide on a virgin metallic beam under bending to heterogeneous synthetic sports equipment design. As such, there are many applications in solid mechanics encompassing weak discontinuities, where efficient computational methods are required to deal with the discontinuous nature of the solution, without the need for fine finite element discretisation in the vicinity of the discontinuity. The numerical approach used to deal with such situations i.e. the displacement-based finite element method, require adjustment in order to meet the needs of potential for complex numerical artefacts such as overstiff behaviour to emerge as a result of inconsistent kinematic assumptions.

While in practice, the displacement-based finite element formulation is used most frequently, other techniques have also been employed successfully and are, in some cases, more efficient. Some very general finite element formulations are obtained by using variational principles that can be regarded as extensions of the principle of stationarity of total potential energy. These extended variational principles use not only the displacements but also the strains and/or stresses as primary variables and lead to what is referred to as mixed finite element formulations. A large number of mixed finite element formulations have been proposed, including that offered by of Kardestuncer and Norrie [1] and the work of Brezzi and Fortin [2]. It has been shown that the Hu-Washizu variational formulation may be regarded as a generalisation of the principle of virtual displacements, in which the displacement boundary conditions and strain compatibility conditions have been relaxed but then imposed by Lagrange multipliers and variations are performed on all unknown displacements, strains, stresses, body forces, and surface tractions.

Mixed finite element discretisation can offer some advantages in certain analyses, compared to the standard displacement-based discretisation. There are two areas in which the use of mixed elements is much more efficient than the use of pure displacement-based elements. These two areas are the analysis of almost incompressible media and the analysis of plate and shell structures. Simpler geometries such as beams can also be studied using the mixed methods and there are advantages in so doing.

The work presented concerns the development of a mixed finite element formulation for the analysis of discontinuous Timoshenko beam and Mindlin-Reissner plate. The basic assumption in the Euler-Bernoulli theory of shallow beams excluding shear deformation is that a normal to the midsurface (neutral axis) of the beam remains normal during deformation and therefore its angular rotation is equal to the slope of the beam midsurface i.e. the first derivative of the lateral displacement field. This kinematic assumption leads to the well-known beam bending governing differential equation in which the transverse displacement is the only variable and requires shape functions that are C^1smooth. Considering now the effect of shear deformations, one retains the assumption that a plane section originally normal to the neutral axis remains plane, but not necessarily normal to the neutral axis. Adopting this

kinematic assumption leads to Timoshenko theory of beams in which the total rotation of the plane originally normal to the neutral axis is given by the rotation of the tangent to the neutral axis and the shear deformation. While Timoshenko beam theory asymptotically recovers the classical theory for thin beams or as the shear rigidity becomes very large and allows the utilization of C^0smooth functions in the finite element formulation, it may be accompanied by erroneous shear strain energy and very small lateral displacements if field-inconsistent finite element formulation is used to solve the governing differential equation. Higher order theories as third-order (e.g. [3] and [4]) or zeroth-order shear deformation theories [5] have also been discussed in the literature and could coalesce with either of the aforementioned theories as limiting cases. In 2D problems plate and shell formulations are extensively used to evaluate thin-walled structures such as aircraft fuselage exposed to bending and pressure loads. The Mindlin-Reissner plate theory is attractive for the numerical simulation of weak and strong discontinuities for several reasons. One major advantage is that Mindlin-Reissner theory enables one to include the transverse shear strains through the thickness in the plate formulation compared to Kirchhoff theory.

When analysing a structure or an element using Timoshenko beam or Mindlin-Reissner plate theory by the virtue of the assumptions made on the displacement field, the shearing deformations cannot be zero everywhere (for thin structures or elements), therefore, erroneous shear strain energy (which can be significant compared with the bending energy) is included in the analysis. This error results in much smaller displacements than the exact values when the beam structure analysed is thin. Hence, in such cases, the finite element models are over-stiff. This phenomenon is observed in the two-noded beam element, which therefore should not be employed in the analysis of thin beam structures, and the conclusion is also applicable to the purely displacement-based low order plate and shell elements. The over-stiff behaviour exhibited by thin elements has been referred to as element shear locking.

Various formulations have been proposed to address the overstiff behaviour exhibited by thin beam [6] and plate [7] elements , referred to as shear locking. In this paper an effective beam element is obtained using a mixed interpolation of displacements and transverse shear strains based on Hellinger-Reissner (HR) functional. The mixed interpolation proposed is an application of the more general procedure employed in the formulation of plate bending and shell elements and is very reliable in that it does not lock, shows excellent convergence behaviour, and does not contain any spurious zero energy modes. In addition, the proposed formulation possesses an attractive computational feature.

In the case of the Timoshenko beam, the stiffness matrices of the elements can be evaluated efficiently by simply integrating the displacement-based model with N Gauss integration point for the $(N+1)$-noded element. Using one integration point in the evaluation of the two-noded element stiffness matrix, the transverse shear strain is assumed to be constant, and the contribution from the bending deformation is still evaluated exactly. In the case of the Mindlin-Reissner plate, Bathe and Dvorkin [8] introduced a general four-noded nonlinear shell element, which was later reduced to a four-noded linear plate bending element for the linear elastic analysis of plates. In their work it was shown how the general continuum mechanics based shell element formulation [9] can be reduced to an interesting plate bending

element. The proposed elements by Bathe and Dvorkin [8] satisfy the isotropy and convergence requirements [10] and also as it has been shown in [9] the transverse displacement and section rotations have been interpolated with different shape functions than the transverse shear strains. The order of shape functions used for interpolating the transverse shear strain is less than the order of shape function used for interpolation of transverse displacement and section rotations.

The method proposed in this study captures the discontinuous nature of solution arising from jump in material properties using the extended finite element method (XFEM) which falls within the framework of the partition of unity method (PUM) [11]. While there is literature galore on the study of strong discontinuities using XFEM (e.g. modelling fracture in Mindlin-Reissner plates [12], cohesive crack growth [13], modelling holes and inclusions [14], analysis of a viscoelastic orthotropic cracked body [15], etc.), there are few studies on using this method to capture the discontinuity for thin plates or beams that do not exhibit shear locking. To mention some recent contributions in this regard, Xu et al. [16] adopted a 6-noded isoparametric plate element with the extended finite element formulation to capture the elasto-plastic behaviour of a plate in small-deformation analyses. The XFEM is used (by enriching the displacement field only which is referred to, herein, as the traditional XFEM [17]) to capture the behaviour of a plate with a locally non-smooth displacement field, and a displacement field with a high gradient. Natarajan et al. [18] studied the effect of local defects, viz., cracks and cut-outs on the buckling behaviour of plates with a functionally graded material subjected to mechanical and thermal loads. The internal discontinuities, i.e. cracks and cut-outs are represented independent of the mesh within the framework of the extended finite element method and an enriched shear flexible 4-noded quadrilateral element is used for spatial discretisation. Van der Meer [19] proposed a level set model that was used in conjunction with XFEM for modelling delamination in composites. Peng [20] considered the fracture of shells with continuum-based shell elements using the phantom node version of XFEM. Baiz et al. [21] studied the linear buckling problem for isotropic plates using a quadrilateral element with smoothed curvatures and the extended finite element method and Larsson et al. [22] studied the modelled dynamic fracture in shell structures using XFEM.

In the present study XFEM is used in conjunction with Mixed Interpolated Tensorial Component (MITC) Timoshenko beam and Mindlin-Reissner plate formulations proposed by Bathe and Dvorkin [8]. MITC has been successful in dealing with the problem of shear locking and has several advantages over displacement-based finite element method. Moysidis et al. [23] implemented a hysteretic plate finite element for inelastic, static and dynamic analysis where s smooth, 3D hysteretic rate-independent model is utilized generalizing the uniaxial Bouc-Wen model. This is expressed in tensorial form, which incorporates the yield criterion and a hardening rule. The elastic mixed interpolation of tensorial components with elements possessing four nodes (MITC4) is extended by considering, as additional hysteretic degrees-of-freedom, the plastic strains at the Gauss integration points of the interface at each layer. Plastic strains evolve following Bouc-Wen equations. Jeon et al. [24] developed a scheme to enrich the 3-noded triangular MITC shell finite element by interpolation cover functions and Ko et al. [25] proposed a new reliable and efficient 4-noded quadrilateral

element, referred to in this study as the 2D-MITC4 element, for two-dimensional plane stress and plane strain solutions of solids using the MITC method.

The proposed method, unlike the conventional XFEM where only the displacement field is enriched, also enriches the transverse shear strains. This method is promising, as have been its counterparts in dealing with the issue of shear locking. For instance, Xu et al. [26] proposed a 6-noded triangular Reissner-Mindlin plate MITC6 element (to mitigate shear locking in both the smooth and the locally non-smooth displacement fields) with XFEM formulation for yield line analyses where regularized enrichment is employed to reproduce a displacement field with a locally high gradient in the vicinity of a yield line in plate structures. There has, however, been minimum research conducted on combining the two methodologies with enriching both the displacement field and the assumed through-thickness strain fields. The proposed method is put to test by solving several benchmark problems and a comprehensive study of results encompassing errors and L_2-norms is provided.

This paper is organised as follows: In sections 2 and 3 the weak formulation of the discontinuous Timoshenko beam and Mindlin-Reissner plate are introduced, respectively, and the governing equations are derived based on the Hellinger-Reissner functional. In section 4 the new XFEM-based (MITC) Timoshenko beam and Mindlin-Reissner plate are developed. The enriched stiffness matrix is evaluated in section 5. Section 6 deals with the use of a numerical technique to evaluate the integrals in the weak formulation. A few case studies have been carried out to examine the robustness of the method in section 7. The summary of the results with respect to analyses conducted and the conclusions of the study are included in section 8.

2. Weak formulation of the Timoshenko beam

As discussed previously both the displacement and strain fields are variables used to derive the governing equations in weak form. To do so, the Hellinger-Reissner functional has been adopted in this work,

$$\Pi_{HR}(\boldsymbol{u},\boldsymbol{\varepsilon}) = \int (-\frac{1}{2}\boldsymbol{\varepsilon}^T\boldsymbol{C}(\boldsymbol{x})\boldsymbol{\varepsilon} + \boldsymbol{\varepsilon}^T\boldsymbol{C}(\boldsymbol{x})\boldsymbol{\partial_\varepsilon}\boldsymbol{u} - \boldsymbol{u}^T\boldsymbol{f}^B)dV \underbrace{- \int \boldsymbol{u}^{S_f^T}\boldsymbol{f}^{S_f} dS - \int \boldsymbol{f}^{S_u T}(\boldsymbol{u}^{S_u} - \boldsymbol{u}_p)dS}_{Boundary\ Terms} \quad (1)$$

With boundary conditions:

$$\boldsymbol{u}^{S_u} = \boldsymbol{u}_p \quad \text{and} \quad \delta\boldsymbol{u}_p = 0 \quad (2)$$

where,

$$\boldsymbol{u} = \begin{bmatrix} u \\ w \end{bmatrix} = \begin{bmatrix} -z\theta \\ w \end{bmatrix}, \boldsymbol{\varepsilon} = \boldsymbol{\partial_\varepsilon}\boldsymbol{u}, \boldsymbol{\tau} = \boldsymbol{C}(\boldsymbol{x})\boldsymbol{\varepsilon}, \boldsymbol{\partial_\varepsilon}\boldsymbol{u} = \begin{bmatrix} \frac{\partial u}{\partial x} \\ \frac{\partial u}{\partial z} + \frac{\partial w}{\partial x} \end{bmatrix} = \begin{bmatrix} \varepsilon_{xx} \\ \gamma_{xz} \end{bmatrix}, \boldsymbol{\varepsilon} = \begin{bmatrix} \varepsilon_{xx} \\ \gamma_{xz}^{AS} \end{bmatrix} \quad (3)$$

$\boldsymbol{\varepsilon}$ is strain tensor field cast in a vector form (including generalised bending strain and assumed shear strain), $\boldsymbol{C}(\boldsymbol{x})$ is the material constitutive tensor, V represents volume, $\boldsymbol{u}$ is a vector containing the displacement field components, $\boldsymbol{f}$ is the force, S represents the surface and $\boldsymbol{\tau}$ is the stress tensor; the subscripts B and S_f represent body and surface, respectively.

This will allow for more control over the interpolation of variables, which will be combined with the mixed interpolation method. The assumptions made are:

1. Constant (along the length up to the point of discontinuity) element transverse shear strain, γ_{xz}^{AS}
2. Linear variation in transverse displacement, w
3. Linear variation in section rotation, θ

Upon substitution of the appropriate variables from equation (3) into equation (1),

$$\Pi_{HR} = \int \left(\frac{1}{2}\varepsilon_{xx}E(x)\varepsilon_{xx} - \frac{1}{2}\gamma_{xz}^{AS}\kappa G(x)\gamma_{xz}^{AS} + \gamma_{xz}^{AS}\kappa G(x)\gamma_{xz} - \boldsymbol{u}^{\mathrm{T}}\boldsymbol{f}^{\mathrm{B}}\right)dV + \text{Boundary Terms} \quad (4)$$

where $E(x)$ represents the Young's modulus at position x, and $G(x)$ represents the shear modulus at the same point, superscript AS denotes the assumed constant value and κ is the shear correction factor taken to be $\frac{5}{6}$, the value which yields correct results for a rectangular cross section and is obtained based on the equivalence of shear strain energies. The degrees-of- freedom are considered to be $\boldsymbol{u}$ and γ_{xz}^{AS}. Invoking $\delta\Pi_{HR} = 0$ and excluding the boundary terms:

1. Corresponding to $\delta\boldsymbol{u}$:

$$\int (\delta\varepsilon_{xx}E(x)\varepsilon_{xx} + \delta\gamma_{xz}\kappa G(x)\gamma_{xz}^{AS})dV = \int \delta\boldsymbol{u}^{\mathrm{T}}\boldsymbol{f}^{\mathrm{B}}\, dV \quad (5)$$

2. Corresponding to $\delta\gamma_{xz}^{AS}$:

$$\int \delta\gamma_{xz}^{AS}\kappa G(x)\left(\gamma_{xz}-\gamma_{xz}^{AS}\right)dV=0 \tag{6}$$

3. Weak formulation of the Mindlin-Reissner plate

Following the same procedures as for the Timoshenko beam, the Hellinger-Reissner functional for the Mindlin-Reissner plate formulation can be derived as:

$$\Pi_{HR}=\frac{1}{2}\int \boldsymbol{\varepsilon_b^T C_b}(\boldsymbol{x})\boldsymbol{\varepsilon_b}\,dV\;-\frac{1}{2}\int \boldsymbol{\varepsilon_s^T C_s}(\boldsymbol{x})\boldsymbol{\varepsilon_s}\,dV\;+ \int \boldsymbol{\varepsilon_s^T C_s}(\boldsymbol{x})\boldsymbol{\partial_{\varepsilon_s}}\boldsymbol{u}\,dV\;-\int \mathbf{u}^{\mathrm{T}}\boldsymbol{f}^{\mathrm{B}}dV\underbrace{-\int \boldsymbol{u}^{S_f^T}\boldsymbol{f}^{S_f}dS\;-\int \boldsymbol{f}^{S_u\,\mathrm{T}}\left(\boldsymbol{u}^{S_u}-\mathbf{u}_{\mathrm{p}}\right)dS}_{\text{Boundary Terms}} \tag{7}$$

This can be used for beam element formulation. The assumptions made are:

1. Constant element transverse shear strains along the edge, $\gamma_{xz_{ij}}^{AS}$ and $\gamma_{yz_{ij}}^{AS}$
2. Linear variation in transverse displacement, w
3. Linear variation in section rotations, θ_x and θ_y

where:

$$\boldsymbol{\partial_{\varepsilon_s}}\boldsymbol{u}=\begin{bmatrix}\frac{\partial \mathrm{u}}{\partial \mathrm{z}}+\frac{\partial \mathrm{w}}{\partial \mathrm{x}}\\ \frac{\partial \mathrm{v}}{\partial \mathrm{z}}+\frac{\partial \mathrm{w}}{\partial \mathrm{y}}\end{bmatrix}=\begin{bmatrix}\gamma_{\mathrm{xz}}\\ \gamma_{\mathrm{yz}}\end{bmatrix},\ \boldsymbol{\partial_{\varepsilon_b}}\boldsymbol{u}=\begin{bmatrix}\frac{\partial \mathrm{u}}{\partial \mathrm{x}}\\ \frac{\partial \mathrm{v}}{\partial \mathrm{y}}\\ \frac{\partial \mathrm{u}}{\partial \mathrm{y}}+\frac{\partial \mathrm{v}}{\partial \mathrm{x}}\end{bmatrix}=\begin{bmatrix}\varepsilon_{\mathrm{xx}}\\ \varepsilon_{\mathrm{yy}}\\ \gamma_{\mathrm{xy}}\end{bmatrix},\ \boldsymbol{\varepsilon_s}=\begin{bmatrix}\gamma_{xz}^{AS}\\ \gamma_{yz}^{AS}\end{bmatrix},\ \boldsymbol{\varepsilon_b}=\begin{bmatrix}\varepsilon_{\mathrm{xx}}\\ \varepsilon_{\mathrm{yy}}\\ \gamma_{\mathrm{xy}}\end{bmatrix},\ \mathbf{u}=\begin{bmatrix}u\\ v\\ w\end{bmatrix}=\begin{bmatrix}-z\theta_x\\ -z\theta_y\\ w\end{bmatrix} \tag{8}$$

Substituting variables above into equation (7),

$$\Pi_{HR}=\int\Big(\varepsilon_x\frac{E(x)}{2(1-\nu^2(x))}\varepsilon_x+\varepsilon_x\frac{E(x)\nu(x)}{(1-\nu^2(x))}\varepsilon_y+\varepsilon_y\frac{E(x)}{2(1-\nu^2(x))}\varepsilon_y+\gamma_{\mathrm{xy}}\frac{E(x)}{4(1+\nu(x))}\gamma_{\mathrm{xy}}-\frac{1}{2}\gamma_{xz}^{AS}\,\kappa\,\mathrm{G(x)}\gamma_{xz}^{AS}-\frac{1}{2}\gamma_{yz}^{AS}\,\kappa\,\mathrm{G(x)}\gamma_{yz}^{AS}+\gamma_{xz}^{AS}\,\kappa\,\mathrm{G(x)}\gamma_{\mathrm{xz}}+\gamma_{yz}^{AS}\,\kappa\,\mathrm{G(x)}\gamma_{\mathrm{yz}}-\boldsymbol{u}^{\mathrm{T}}\boldsymbol{f}^{\mathrm{B}}\Big)dV+\text{Boundary Terms} \tag{9}$$

4. XFEM discretisation

Both FEM and XFEM could be formulated to avert shear locking, however, it is computationally less expensive to incorporate both discontinuity jumps and shear locking free formulations using XFEM. Besides XFEM would allow for the effect of moving interfaces on stress and strain fields without the requirement of re-meshing. The partition of unity allows the standard FE approximation to be enriched in the desired domain, and the enriched approximation field is as follows:

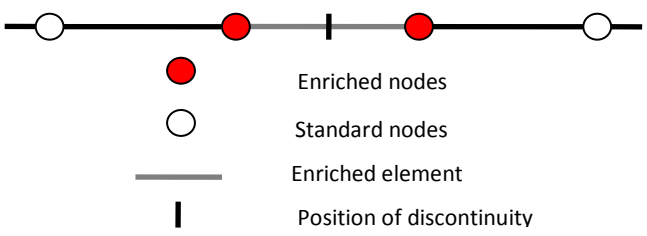


Figure 1. XFEM enrichment implemented in a 1D geometry

$$u_i(\boldsymbol{x}) = \sum_{I \in S} N_I(\boldsymbol{x}) U_{I_i} + \sum_{J \in S^{enr}} M_J(\boldsymbol{x}) \left(\psi(\boldsymbol{x}) - \psi(\boldsymbol{x_J})\right) A_{J_i} \tag{10}$$

Where S^{enr} signifies the domain to be enriched, $M_J(\boldsymbol{x})$ is the J^{th} function of the partition of unity, $\psi(\boldsymbol{x})$ is the enriched or additional function, and A_{J_i} is the additional unknown associated with the $M_J(\boldsymbol{x})$ for the i^{th} component. Figure 1 illustrates the notion of enrichment in a beam.

Note that the orders of N_I and M_J do not have to be the same. For instance, one may use a higher order polynomial for the shape function N_I and a linear shape function for M_J. The advantage of this is one is able to optimise the analysis by imposing different orders of functions in different domains.

It is also important to mention that, in order to track the moving interfaces, the method proposed by Osher and Sethian [26] has been used through the definition of the level set. Furthermore, all the discontinuities considered, are weak discontinuities i.e. the displacement is continuous across the interface but its derivative is not so. Thus, a ramp enrichment will be used for all problems representing such a scenario (inclusions, bi-materials, patches, etc.).

Moës et. al. [27] proposed a new enrichment function which has a better convergence rate than the traditional ramp function:

$$\psi(\boldsymbol{x}) = \sum_J N_J(\boldsymbol{x}) \left|\varphi_J\right| - \left|\sum_J N_J(\boldsymbol{x}) \varphi_J\right| \tag{11}$$

where $N_J(\boldsymbol{x})$ is the traditional standard element shape functions and $\varphi_J = \varphi(\boldsymbol{x_J})$ is the signed distance function. The distance d from point $\boldsymbol{x}$ to the point $\boldsymbol{x_\Gamma}$ on the interface Γ is a scalar defined as:

$$d = \|\boldsymbol{x_\Gamma} - \boldsymbol{x}\| \tag{12}$$

If the outward normal vector $\boldsymbol{n}$ is pointed towards $\boldsymbol{x}$, the distance is at a minimum and the signed distance function is set as $\varphi(\boldsymbol{x})$ defined as:

$$\begin{cases} \varphi(\boldsymbol{x}) = +\min(d) & if \quad \boldsymbol{x} \in \Omega_A \\ \varphi(\boldsymbol{x}) = -\min(d) & if \quad \boldsymbol{x} \in \Omega_B \end{cases} \tag{13}$$

This can be written in a single equation as:

$$\varphi(\boldsymbol{x}) = \min(|\boldsymbol{x_\Gamma} - \boldsymbol{x}|)\, sign(\boldsymbol{n}.(\boldsymbol{x_\Gamma} - \boldsymbol{x})) \tag{14}$$

Figure 2 represents the schematics of the domain under consideration.

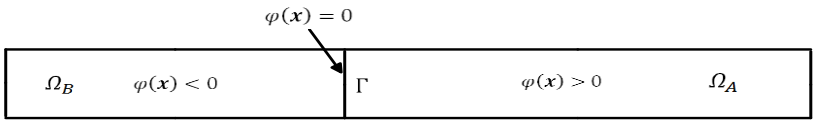


Figure 2. Schematic of the decomposition of the domain to two subdomains and the use of a level set function

The advantage of this enrichment over the ramp function (i.e.$\psi\ (\boldsymbol{x}) = |\varphi(\boldsymbol{x})|$) is that it can be identified immediately, as the nodal value of the enrichment function is zero. This reduces the error produced by the blending elements.

5. The proposed XFEM formulation

5.1. Timoshenko beam element

In this paper the extrinsic enrichment has been adopted. Two types of extrinsic, local enrichment functions are used viz. the standard Heaviside step function, $H(\boldsymbol{x})$, and the ramp functions, $\psi(x)$, from equation (11). The nodal degrees-of-freedom for an enriched linear Timoshenko beam element are of the form:

$$\hat{\boldsymbol{u}} = \begin{bmatrix} w_i \\ \theta_i \\ A_{w_i} \\ A_{\theta_i} \end{bmatrix} \qquad \text{and} \qquad \hat{\boldsymbol{\gamma}} = \begin{bmatrix} \hat{\varepsilon}_k \\ A_{\hat{\varepsilon}_k} \end{bmatrix} \tag{15}$$

Where A_{w_i} and A_{θ_i} are the extra degrees-of-freedom appeared due to the enrichment of elements containing the discontinuity. Also $i = 1,2$ and $k = 1$ for a linear element and $i = 1,2,3$ and $k = 1,2$ for a quadratic element. Therefore, from the classical finite element formulation and for a fully enriched element, the new MITC Timoshenko extended finite element (XFEM) beam formulation is introduced as follows:

$$\boldsymbol{u} = \begin{bmatrix} u \\ w \end{bmatrix} = \begin{bmatrix} -z\theta \\ w \end{bmatrix} = \begin{bmatrix} -z\sum_i N_i\theta_i - z\sum_i N_i\{\psi(x) - \psi(x_i)\}A_{\theta_i} \\ \sum_i N_i w_i \ + \sum_i N_i\{\psi(x) - \psi(x_i)\}A_{w_i} \end{bmatrix} \tag{16}$$

$$\gamma_{xz}^{AS} = \sum_k N_k^* \hat{\varepsilon}_k + \sum_k N_k^* A_{\hat{\varepsilon}_k} H \tag{17}$$

It is important to mention that in the classical XFEM the displacement field is only enriched whereas in the proposed method due to governing equations the strain field is also enriched. Also, the order of the shape functions, N_i^* are one less than the classical shape functions, N_i. As the result of the proposed method the new MITC Timoshenko XFEM formulation in compact form is (with a priori knowledge of the solution included into the XFEM formulation):

$$\boldsymbol{u} = \boldsymbol{H}\hat{\boldsymbol{u}} \quad , \quad \boldsymbol{\gamma_{xz}^{AS}} = \boldsymbol{B_S^{AS}}\hat{\boldsymbol{\gamma}} \quad , \boldsymbol{\gamma_{xz}} = \boldsymbol{B_s}\hat{\boldsymbol{u}} \quad , \quad \boldsymbol{\varepsilon_{xx}} = \boldsymbol{B_b}\hat{\boldsymbol{u}} \tag{18}$$

Where,

$$\boldsymbol{H} = \begin{bmatrix} 0 & -zN_i & 0 & -zN_i\Delta\psi_i \\ N_i & 0 & N_i\Delta\psi_i & 0 \end{bmatrix} \quad , \quad \Delta\psi_i = \psi(x) - \psi(x_i) \tag{19}$$

Where the enrichment functions have been introduced in section 4. The relation between the element nodal degrees-of-freedom and strain can be derived from:

$$\boldsymbol{B_b} = \left[\frac{d\boldsymbol{H_{1j}}}{dx}\right] \quad , \quad \boldsymbol{B_s} = \left[\frac{d\boldsymbol{H_{2j}}}{dx} + \frac{d\boldsymbol{H_{1j}}}{dz}\right] \quad , \quad \boldsymbol{B_S^{AS}} = [N_k^* \quad N_k^* H(\xi)] \tag{20}$$

5.2. Mindlin-Reissner plate element

The same procedure can be followed to formulate the proposed Mindlin-Reissner plate element. Subsequently,

$$\mathbf{u} = \begin{bmatrix} u \\ v \\ w \end{bmatrix} = \begin{bmatrix} -z\theta_x \\ -z\theta_y \\ w \end{bmatrix} = \begin{bmatrix} -z\sum_{i=1}^{4} N_i\theta_{x_i} - z\sum_{j=1}^{N_{en}} N_j\{\psi(x) - \psi(x_j)\}A_{\theta_{x_j}} \\ -z\sum_{i=1}^{4} N_i\theta_{y_i} - z\sum_{j=1}^{N_{en}} N_j\{\psi(x) - \psi(x_j)\}A_{\theta_{y_j}} \\ \sum_{i=1}^{4} N_i w_i + \sum_{j=1}^{N_{en}} N_j\{\psi(x) - \psi(x_j)\}A_{w_j} \end{bmatrix} , \hat{\boldsymbol{u}} = \begin{bmatrix} \theta_{xi} \\ \theta_{yi} \\ w_i \\ A_{\theta_{xi}} \\ A_{\theta_{yi}} \\ A_{w_i} \end{bmatrix} \tag{21}$$

$$\gamma_{xz}^{AS} = \sum_{i=1}^{2} \widehat{N}_i\hat{\gamma}_{xz_i} + \sum_{i=1}^{2} \widehat{N}_i \, \mathrm{H} A_{\hat{\gamma}_{xz_i}} \quad , \quad \gamma_{yz}^{AS} = \sum_{i=1}^{2} \widehat{\widehat{N}}_\imath\hat{\gamma}_{yz_i} + \sum_{i=1}^{2} \widehat{\widehat{N}}_\imath \, \mathrm{H} A_{\hat{\gamma}_{yz_i}} \tag{22}$$

A_{w_i} , $A_{\theta_{x_i}}$, $A_{\theta_{y_i}}$ and $A_{\hat{\varepsilon}_i}$ are the extra (enriched) degrees-of-freedom due to the enrichment of the elements containing the discontinuity. The new proposed MITC4 mixed enrichment Mindlin-Reissner plate formulation using XFEM would be:

$$\boldsymbol{u} = \boldsymbol{H}\hat{\boldsymbol{u}} \quad , \quad \boldsymbol{\varepsilon_b} = \boldsymbol{B_b}\hat{\boldsymbol{u}} \quad , \quad \boldsymbol{\partial_{\varepsilon_s}}\mathbf{u} = \mathbf{B_s}\hat{\boldsymbol{u}} \quad , \quad \boldsymbol{\varepsilon_s} = \boldsymbol{B_S^{AS}}\hat{\boldsymbol{\gamma}} \tag{23}$$

where:

$$\boldsymbol{H} = \left[\begin{array}{ccc|ccc} -zN_i & 0 & 0 & -zN_i\Delta\psi_i & 0 & 0 \\ 0 & -zN_i & 0 & 0 & -zN_i\Delta\psi_i & 0 \\ 0 & 0 & N_i & 0 & 0 & N_i\Delta\psi_i \end{array}\right] , \Delta\psi_1 = \psi(x) - \psi(x_1) \tag{24}$$

Also, the tensors in equation (23) are as follow,

$$\mathbf{B_b} = \begin{bmatrix} \frac{\partial \mathbf{H_{1j}}}{\partial \mathbf{x}} \\ \frac{\partial \mathbf{H_{2j}}}{\partial \mathbf{y}} \\ \frac{\partial \mathbf{H_{1j}}}{\partial \mathbf{y}} + \frac{\partial \mathbf{H_{2j}}}{\partial \mathbf{x}} \end{bmatrix} , \mathbf{B_s} = \begin{bmatrix} \frac{\partial \mathbf{H_{1j}}}{\partial \mathbf{z}} + \frac{\partial \mathbf{H_{3j}}}{\partial \mathbf{x}} \\ \frac{\partial \mathbf{H_{2j}}}{\partial \mathbf{z}} + \frac{\partial \mathbf{H_{3j}}}{\partial \mathbf{y}} \end{bmatrix} , \boldsymbol{B_S^{AS}} = \left[\begin{array}{cccc|cccc} \widehat{N}_1 & \widehat{N}_2 & 0 & 0 & \widehat{N}_1 H & \widehat{N}_2 H & 0 & 0 \\ 0 & 0 & \widehat{\widehat{N}}_1 & \widehat{\widehat{N}}_2 & 0 & 0 & \widehat{\widehat{N}}_1 H & \widehat{\widehat{N}}_2 H \end{array}\right] \tag{25}$$

6. Stiffness matrix evaluation

The Mindlin-Reissner plate formulation stiffness matrix and force vectors can be evaluated through substitution of equation (23) into equations (9),

$$\begin{bmatrix} \boldsymbol{K_{uu}} & \boldsymbol{K_{u\varepsilon}} \\ \boldsymbol{K_{u\varepsilon}^T} & \boldsymbol{K_{\varepsilon\varepsilon}} \end{bmatrix} \begin{bmatrix} \widehat{\boldsymbol{u}} \\ \widehat{\boldsymbol{\gamma}} \end{bmatrix} = \begin{bmatrix} \boldsymbol{R_B} \\ \mathbf{0} \end{bmatrix} \tag{26}$$

where:

$$\boldsymbol{K_{uu}} = \int \mathbf{B_b^T}\, \boldsymbol{C_b}(\boldsymbol{x}) \mathbf{B_b} dV \quad , \quad \boldsymbol{K_{u\varepsilon}} = \int \mathbf{B_s^T}\, \kappa \boldsymbol{C_s}(\boldsymbol{x}) \mathbf{B_s^{AS}} dV \tag{27}$$

$$\boldsymbol{K_{\varepsilon\varepsilon}} = -\int \left(\mathbf{B_s^{AS}}\right)^{\mathbf{T}} \kappa\, \boldsymbol{C_s}(\boldsymbol{x}) \mathbf{B_s^{AS}} dV \quad , \quad \boldsymbol{R_B} = \int \mathbf{H^T} \boldsymbol{f}^{\mathrm{B}}\, dV \tag{28}$$

To reduce the number of degrees-of-freedom and therefore reduce the computational cost the stiffness matrix in equation (26) can be reduced to:

$$\boldsymbol{Ku} = \boldsymbol{R_B} \quad \text{where} \quad \boldsymbol{K} = \boldsymbol{K_{uu}} - \boldsymbol{K_{u\varepsilon}} \boldsymbol{K_{\varepsilon\varepsilon}^{-1}} \boldsymbol{K_{u\varepsilon}^T} \tag{29}$$

The stiffness matrix and force vector of Timoshenko beam element can be derived by substituting, $\boldsymbol{C_b}(\boldsymbol{x}) = E(x)$ and $\boldsymbol{C_s}(\boldsymbol{x}) = G(x)$ in equations (27) and (28).

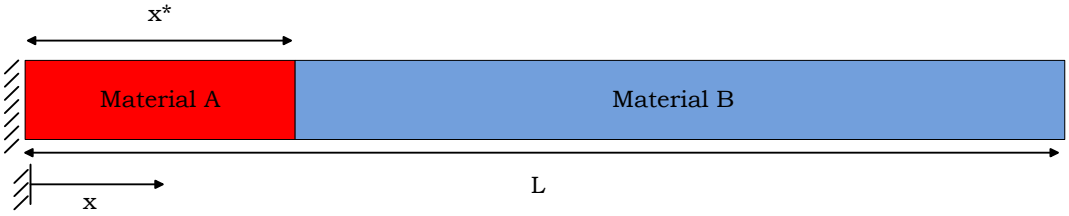
7. Case studies

In this section, results of different models are presented, and the results of proposed XFEM are compared with the analytical solutions derived and numerical results obtained by ABAQUS 6.12/FEM using reduced integration technique to avoid locking. All the results are analysed in detail for convergence and accuracy.

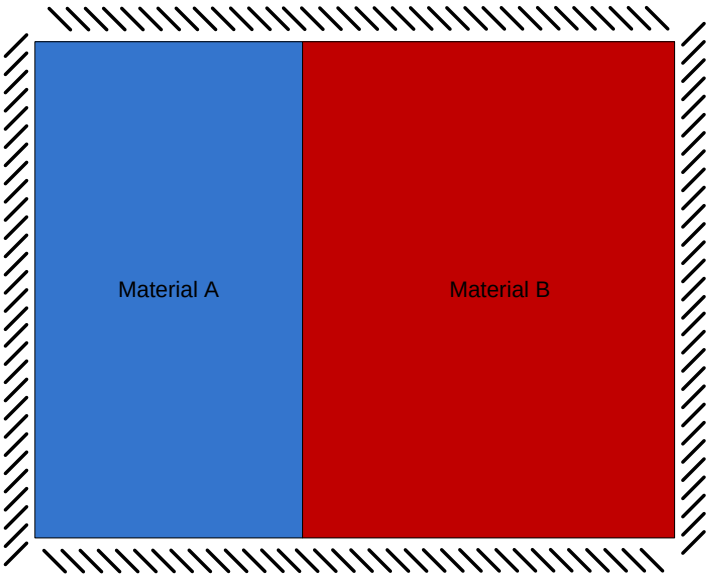
7.1. Problem definition

Considering the schematic of a cantilever bi-material Timoshenko beam (shown in Figure 3a) the analytical solutions (i.e. displacement and through-thickness strain fields) for a Timoshenko beam under different loadings are derived (equations (*A10)-(A15)* in Appendix A). The analytical solution for Timoshenko beam is used to demonstrate the robustness of the proposed XFEM formulation when compared to the traditional XFEM and FEM.

Furthermore, the model is adopted for derivation of enrichment functions used in XFEM. Analogously, a discontinuous plate (shown in Figure 3b) could be studied using the proposed method.



(a)



(b)

Figure 3. (a) Schematic of a cantilever bi-material with arbitrarily positioned point of discontinuity, (b) Discontinuous Mindlin-Reissner plate.

7.2. Timoshenko beam

In this section, the discontinuous Timoshenko beam will be considered.

7.2.1. Simple cantilever beam under uniformly distributed load

The geometric dimensions are as defined in Figure 3 and the following values are assigned to them. The associated material properties are shown in Table 1:

variable	ν_A	$E_A[Kgm^{-1}s^{-2}]$	$G_A[Kgm^{-1}s^{-2}]$	ν_B	$E_B[Kgm^{-1}s^{-2}]$	$G_B[Kgm^{-1}s^{-2}]$
value	0.3	$2x10^5$	$E_A/2(1+\nu_A)$	0.25	$2x10^4$	$E_B/2(1+\nu_B)$

Table 1. Material properties

In this section the static response of a discontinuous Timoshenko beam made of linear elements subjected to a uniformly distributed load (UDL) of magnitude P_0 is studied. The

results shown in Figures 4-9 (plots left) concern the proposed XFEM formulation and the results extracted from the traditional XFEM have been shown in Figures 4-9 (right).

Figures 4-7 are the results of displacements and shear strains when only 9 elements are used along the beam. Figures 4 (left) and 5 (left) show that the proposed XFEM displacements are in good correlation with the analytical solution. In addition to that, the proposed XFEM captures the jump in strains across the discontinuity more accurate than the traditional XFEM where only the displacement field is enriched; this has clearly been shown in Figures 6 and 7. Finally Figures 8 and 9 show that the proposed XFEM converges faster to the exact solution than the traditional XFEM.

All the results obtained in this section suggest that the proposed XFEM (where both the displacement and shear strain are enriched with mixed enrichment functions) gives a better result for displacement and the strain fields and as a consequence of that the method has a better rate of convergence when compared with the traditional XFEM where only the displacement field is enriched.

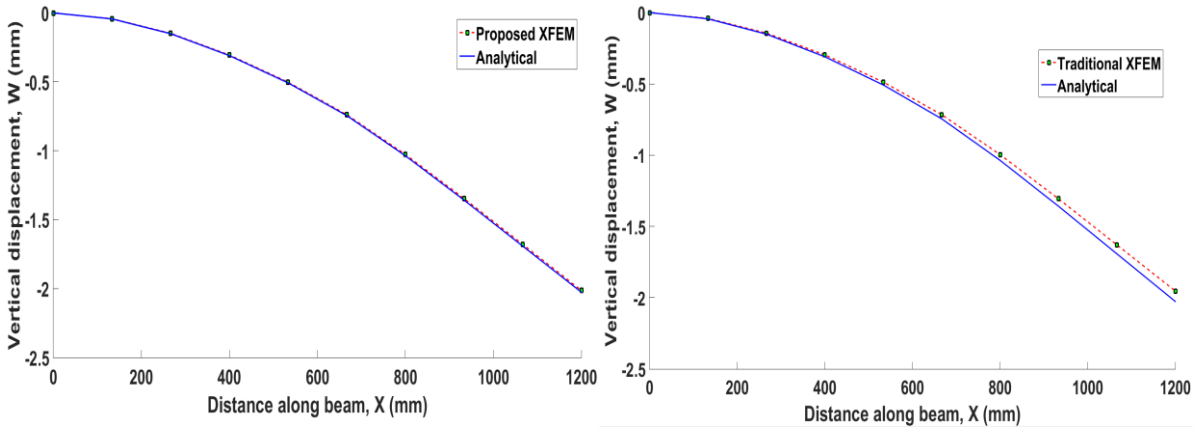


Figure 4. Comparison of vertical displacements, *w* of proposed XFEM (Left) and Traditional XFEM (right) vs analytical solution for linear elements under UDL

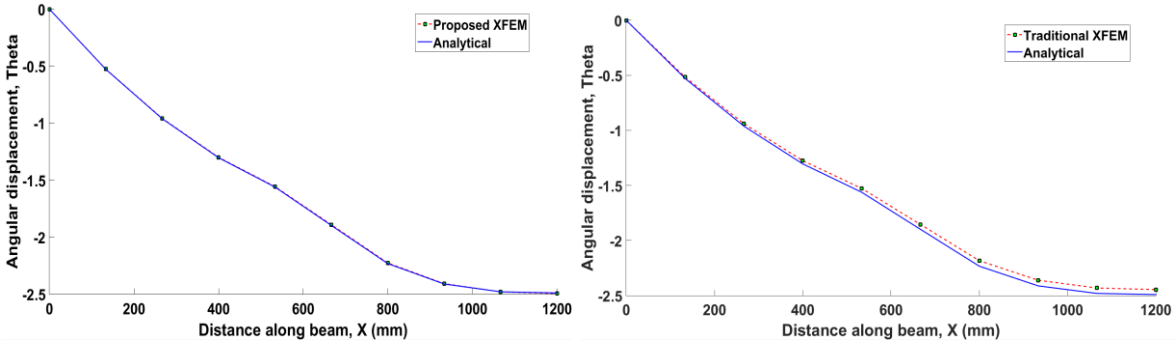


Figure 5. Comparison of section rotation θ of proposed XFEM (Left) and Traditional XFEM (right) vs. analytical solution for linear elements under UDL

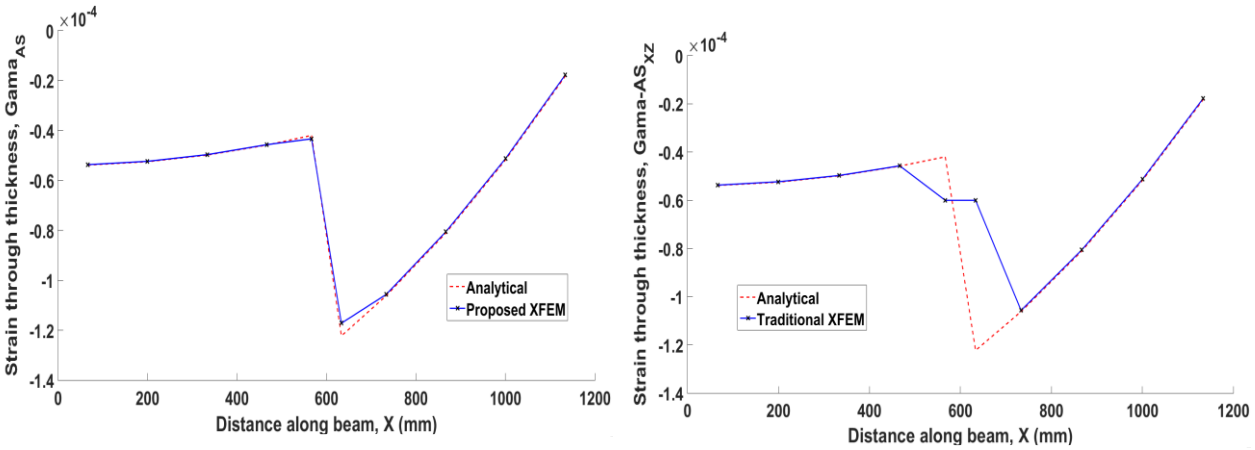


Figure 6. Comparison of shear strain γ_{xz} of proposed XFEM (Left) and Traditional XFEM (right) vs. analytical solution for linear elements under UDL

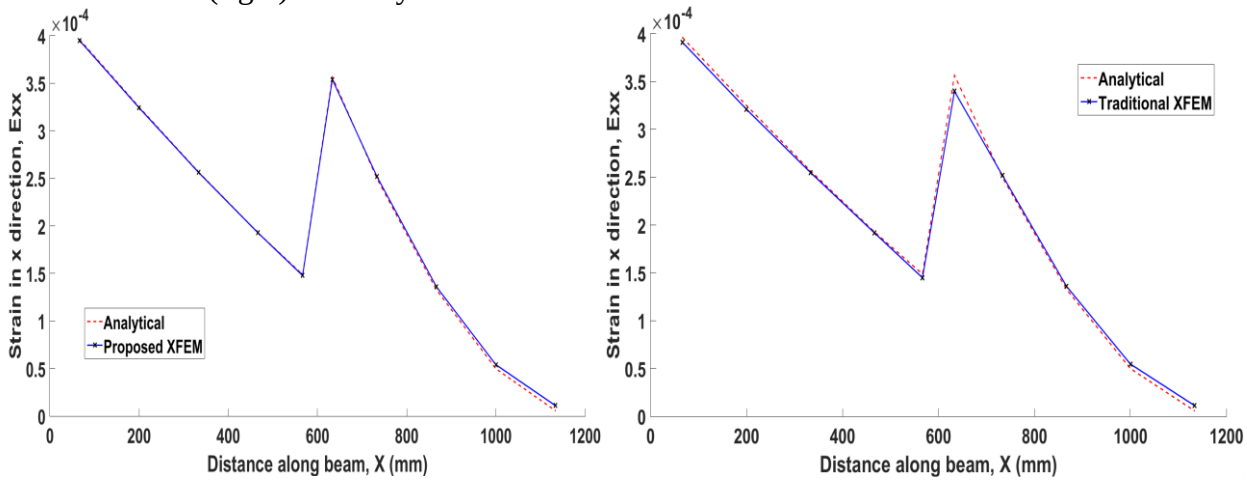


Figure 7. Comparison of direct strain ε_{xx} in x direction of proposed XFEM (Left) and Traditional XFEM (right) vs analytical solution for linear elements under UDL

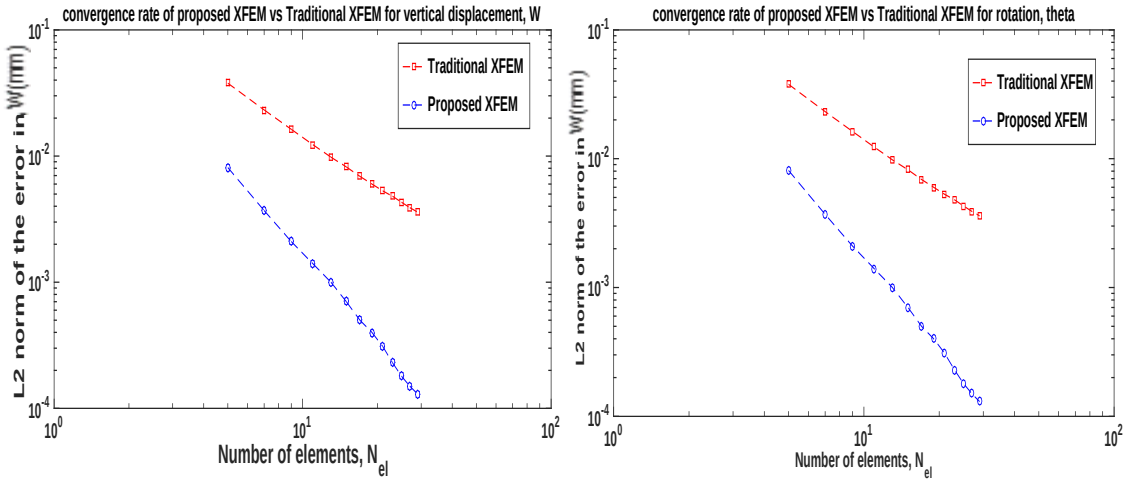


Figure 8. Rate of convergence of vertical displacement (w) (left) and rotation (θ) (right) of traditional XFEM vs proposed XFEM for linear elements under UDL

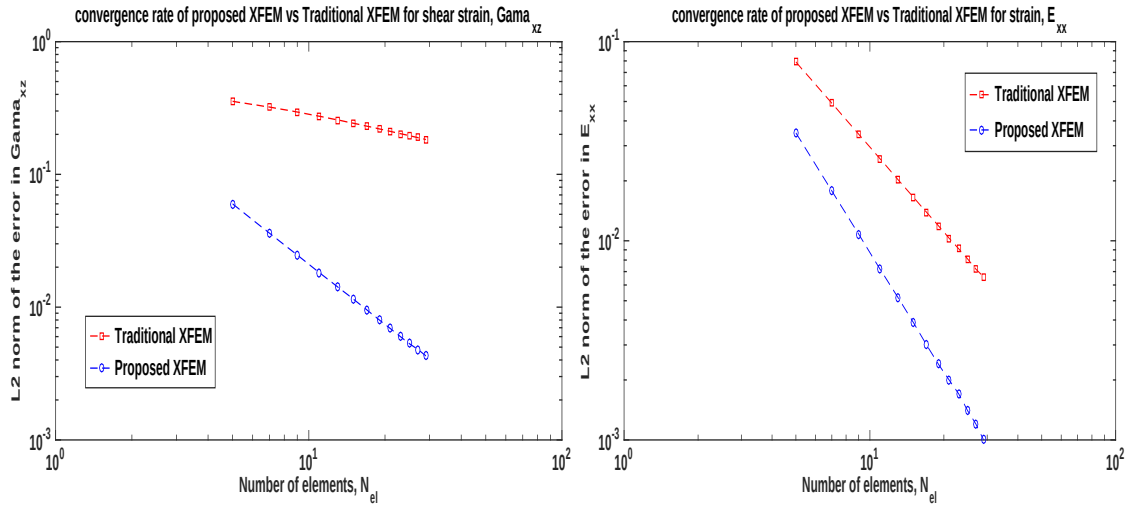


Figure 9. Rate of convergence of shear strain (γ_{xz}) (left) and direct strain in x direction (ε_{xx}) (right) of traditional XFEM vs proposed XFEM for linear elements under UDL

The authors now look into the convergence of static response for the Timoshenko beam subjected to UDL of magnitude P_0 and linearly varying loading of maximum magnitude P_0 using both linear and quadratic elements. Geometric parameters are, as before, in Figure 3, and the material properties are shown in Table 2 as follows:

$$L = 1200\ (mm), h = 200(mm), d = 100(mm), x^* = 600\ (mm), P_0 = 1(Kgm^{-1}s^{-2})$$

variable	ν_A	$E_A[Kgm^{-1}s^{-2}]$	$G_A[Kgm^{-1}s^{-2}]$	ν_B	$E_B[Kgm^{-1}s^{-2}]$	$G_B[Kgm^{-1}s^{-2}]$
value	0.25	$2x10^5$	$E_A/2x(1+\nu_A)$	0.34	$6.83x10^4$	$E_B/2x(1+\nu_B)$

Table 2. Material properties

The results have been shown in Figures 10 and 11 for UDL and in Figures 12 and 13 for linear loading. They illustrate clearly that XFEM formulation converges to the exact solution with a higher rate of convergence than the classical FEM.

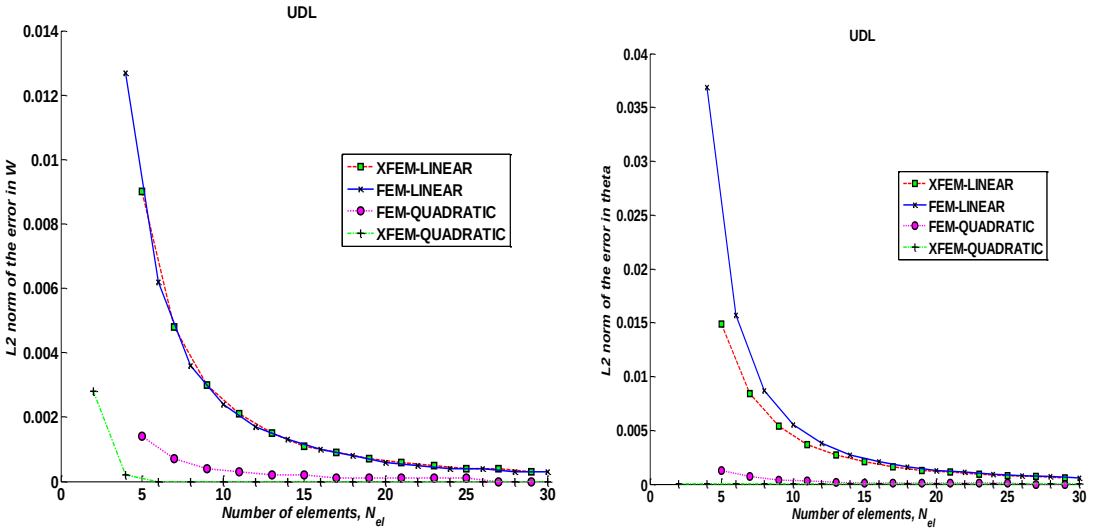


Figure 10. Comparison of convergence of proposed XFEM vs FEM for vertical displacement (left) and rotation (right) for linear and quadratic elements under UDL

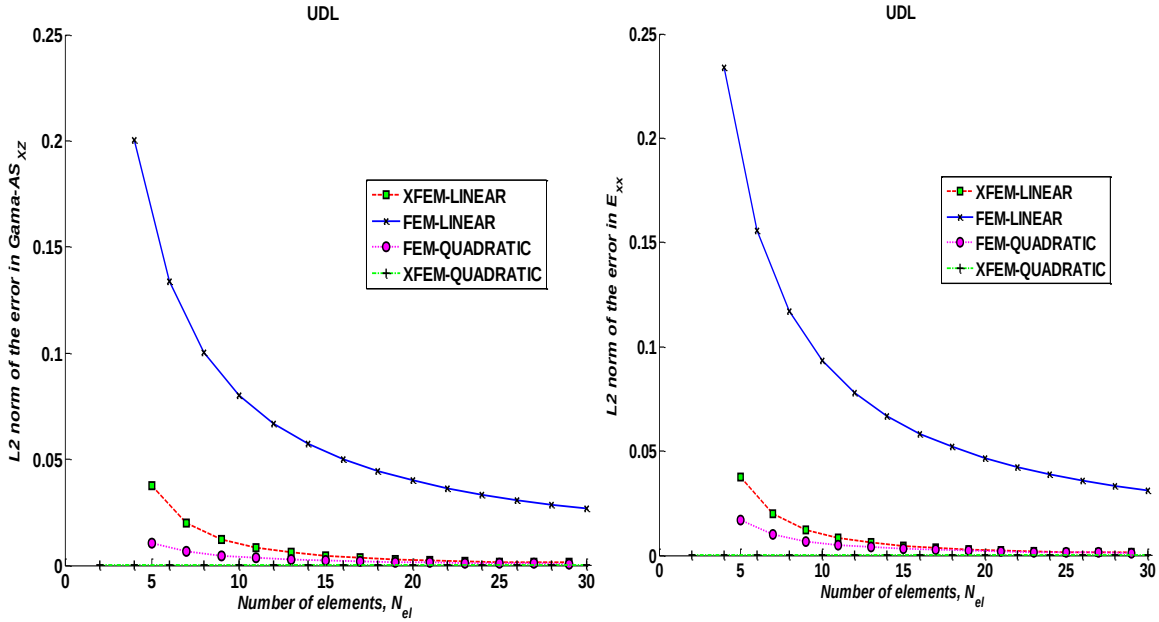


Figure 11. Comparison of convergence of proposed XFEM vs FEM for shear strain (γ_{xz}) (left) and direct strain in x direction (ε_{xx}) (right) for linear and quadratic elements under UDL

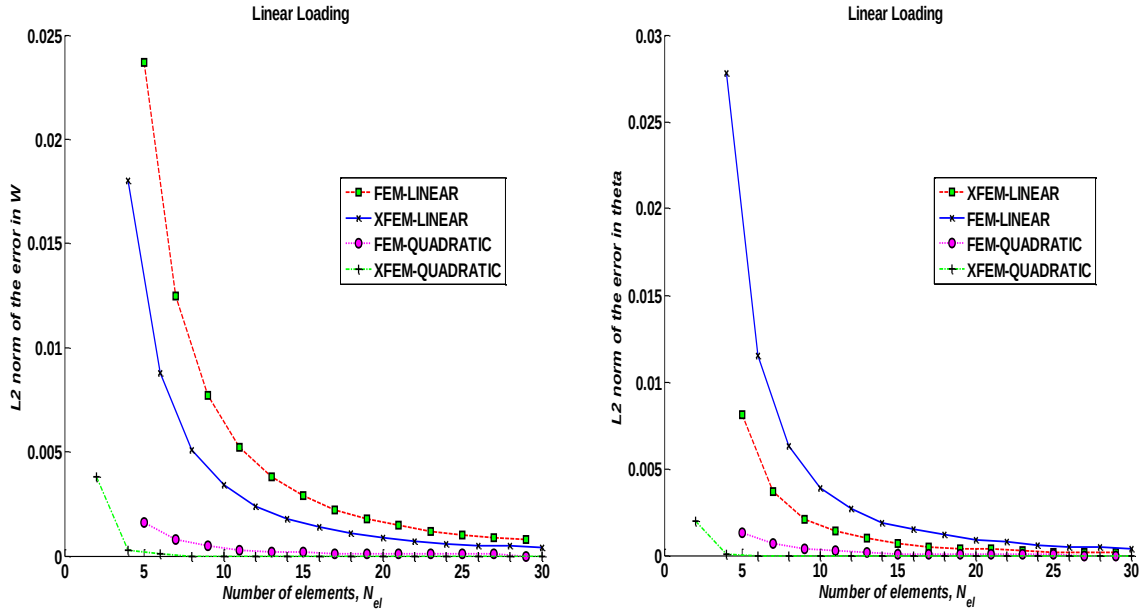


Figure 12. Comparison of convergence of proposed XFEM vs FEM for vertical displacement (w) (left) and rotation (θ) (right) for linear and quadratic elements under linear loading

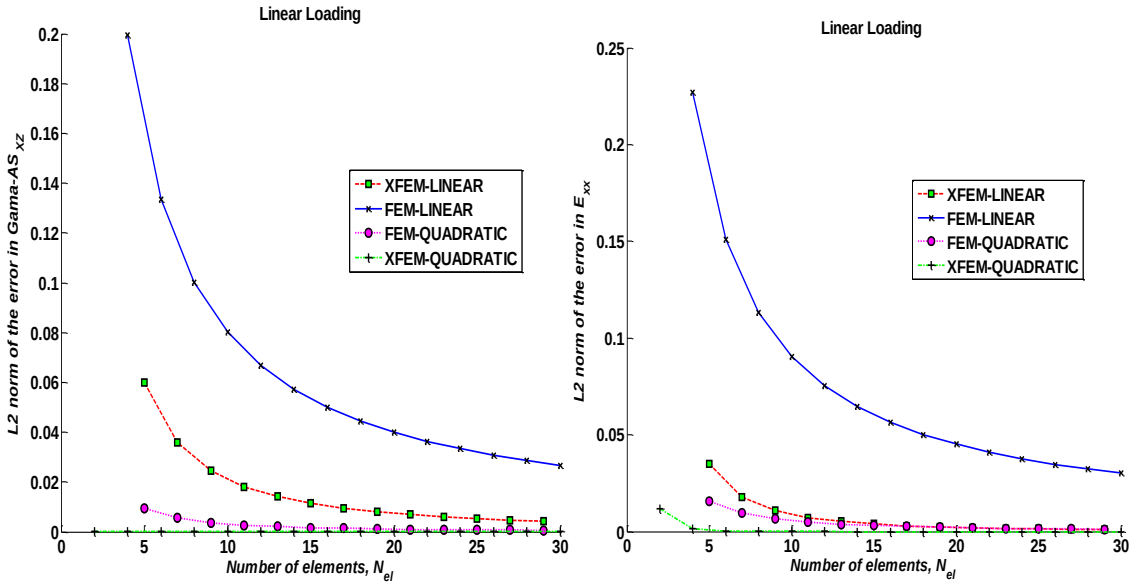


Figure 13. Comparison of convergence of proposed XFEM vs FEM for shear strain (γ_{xz}) (left) and strain in x direction (ε_{xx}) (right) for linear and quadratic elements under linear loading

7.2.2. Bi-material cantilever beam under pure bending

In order to obtain further insight into the behaviour of the proposed XFEM element formulation as the beam grows thin, a bi-material cantilever beam under pure bending has been considered (Figure 14).

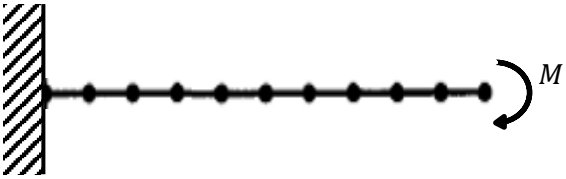


Figure 14. Schematics of a cantilever beam with n equally spaced elements under pure bending due to a concentrated tip moment

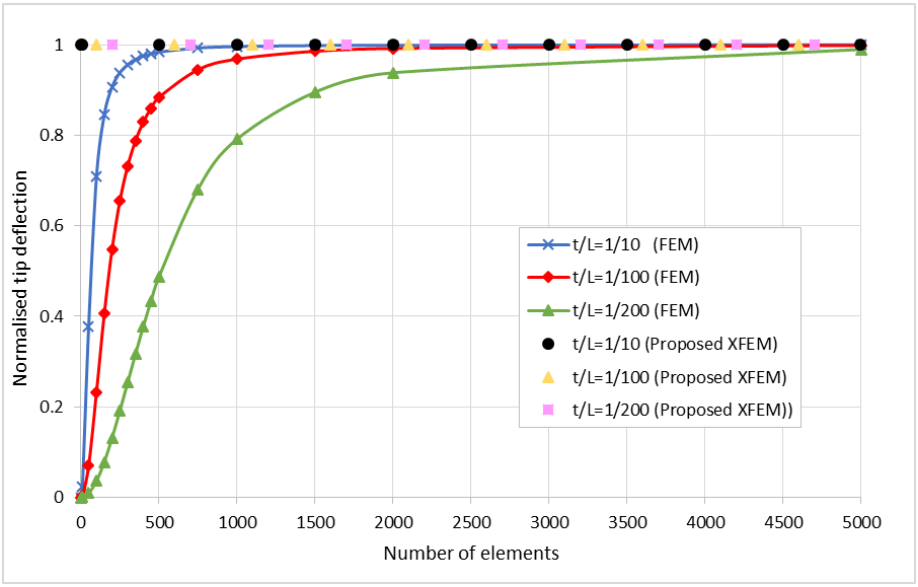


Figure 15. Solution of cantilever beam problem under pure bending. Normalised tip deflection vs. the number of elements used, showing locking of standard elements. In all cases linear elements are used.

Through using the classical principle of virtual work (adopting Timoshenko beam formulation), it can be shown that as the beam grows thin the constraint of zero shear deformations will be approached. This argument holds for the actual continuous model which is governed by the stationarity of the total potential energy in the system. Considering now the finite element representation, it is important that the finite element displacement and/or shear assumptions admit small shear deformation throughout the domain of the thin beam element. If this is not satisfied then an erroneous shear strain energy is included in the analysis. This error results in much smaller displacements than the exact values when the beam structure analysed is thin. Hence, in such cases, the finite element models are much too stiff (element shear locking).

To demonstrate this phenomenon quantitatively, linear beam elements are used to study the robustness of the element formulation in alleviating shear locking for very think structures. As a result a cantilever beam has been studied where the thickness of the beam is reduced substantially $\left({}^{t}/_{L} = 0.5,\ {}^{t}/_{L} = 0.01 \text{ and } {}^{t}/_{L} = 0.002\right)$. The deflection at the free end (i.e. tip of the beam) has been used as the reference value to compare different results obtained.

Material properties, applied moment and the dimensions of the squared cross section of the beam are as follows:

$$M = 1000\ (N), L = 10\ (m), x^* = 5\ (m), E_1 = 100\ (GPa), \nu_1 = 0.25, E_2 = 85\ (GPa), \nu_2 = 0.3$$

The results in Figure 15 (the solutions are normalised with the analytical solution derived for the bi-material beam in this paper) demonstrate that when applying classical (displacement-based finite element) linear Timoshenko elements for modelling very thin cantilever beams, shear locking is observed whereas in the proposed XFEM this problem is alleviated.

7.3. Mindlin-Reissner plate

In this section the Mindlin-Reissner plate has been considered. First, a fully-clamped discontinuous square plate with stationary location of discontinuity under uniform pressure has been analysed under static loading. Secondly, a circular fully-clamped plate with moving discontinuity subject to a central concentrated load is analysed. As a final example, a rectangular plate with radially sweeping discontinuity front has been considered. In all cases the results of the proposed XFEM have been compared with ABAQUS/ FEM using the reduced integration technique to avoid shear locking.

7.3.1. Fully-clamped square plate under uniform pressure

The geometric dimensions and boundaries of the plate under investigation have been shown in Figure 16. The following values are assigned to them, and the associated material properties are shown in Table 3:

$$a = 1\ (m), b = 1\ (m), h = 0.05\ (m), x^* = 0.5\ (m), P_0 = 1.0\text{x}10^4 (Kgm^{-1}s^{-2})$$

Variable	ν_1	$E_1[kgm^{-1}s^{-2}]$	$G_1[kgm^{-1}s^{-2}]$	ν_1	$E_1[kgm^{-1}s^{-2}]$	$G_1[kgm^{-1}s^{-2}]$
Value	0.25	2×10^5	$E_1/2\times(1+\nu_1)$	0.3	2×10^4	$E_1/2\times(1+\nu_1)$

Table 3. Material properties of static fully clamped plate under uniform pressure

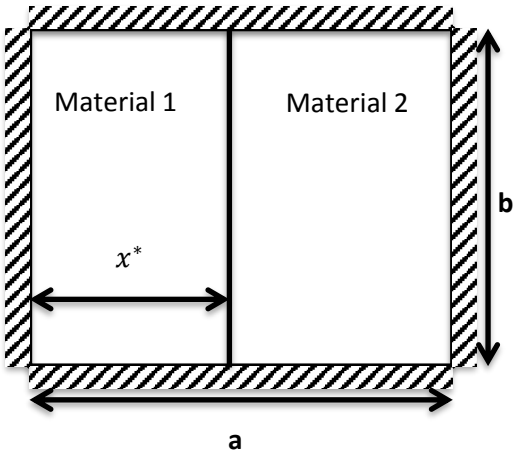


Figure 16. Schematic of a fully clamped plate with arbitrarily positioned point of discontinuity

In this section the static response of the plate made of linear elements subjected to a uniform pressure of magnitude P_0 is considered. The results are shown in Figures below concerning the proposed XFEM formulation against the results from ABAQUS/classical Mindlin-Reissner reduced integration FEM.

Figures 18-21 are the results of displacements and strain. All of the results are taken along the line $y = 0.5$. Figure 17 shows the domain is meshed using standard FEM and XFEM.

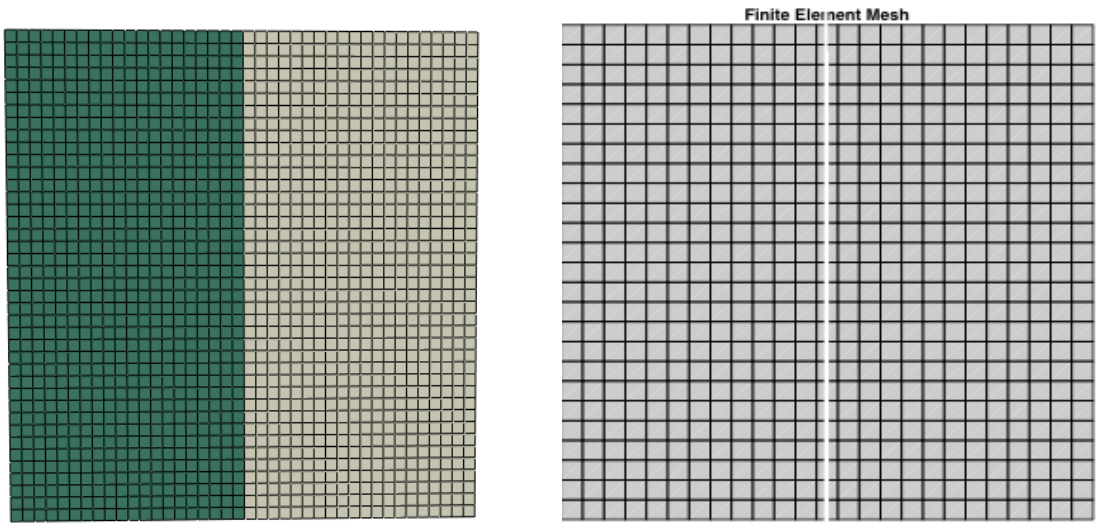


Figure 17. Typical standard FE mesh (left) and XFEM mesh (right)

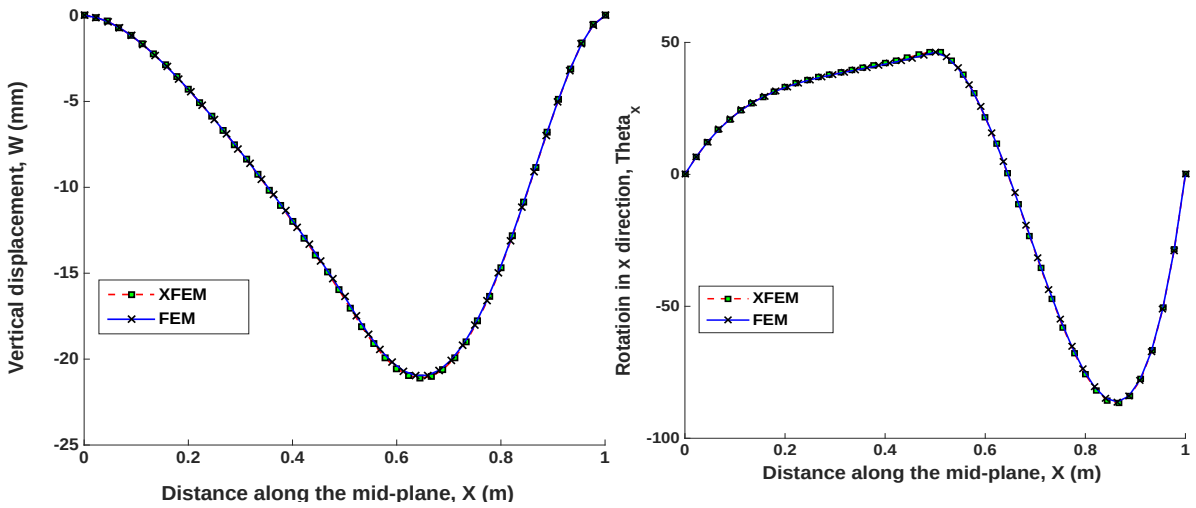


Figure 18. Comparison of vertical displacement (w) (left) and section rotation about y-axis θ_x (right) of proposed XFEM vs. FEM/ABAQUS using reduced integration technique

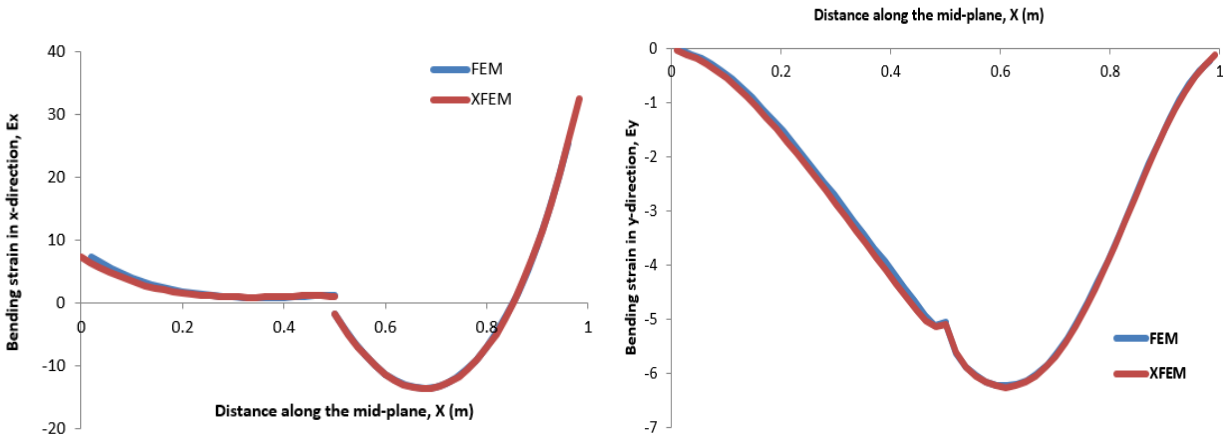


Figure 19. Comparison of bending strain in x-direction, ε_x (left) and bending strain in y-direction, ε_y (right) of proposed XFEM vs. FEM/ABAQUS using reduced integration technique

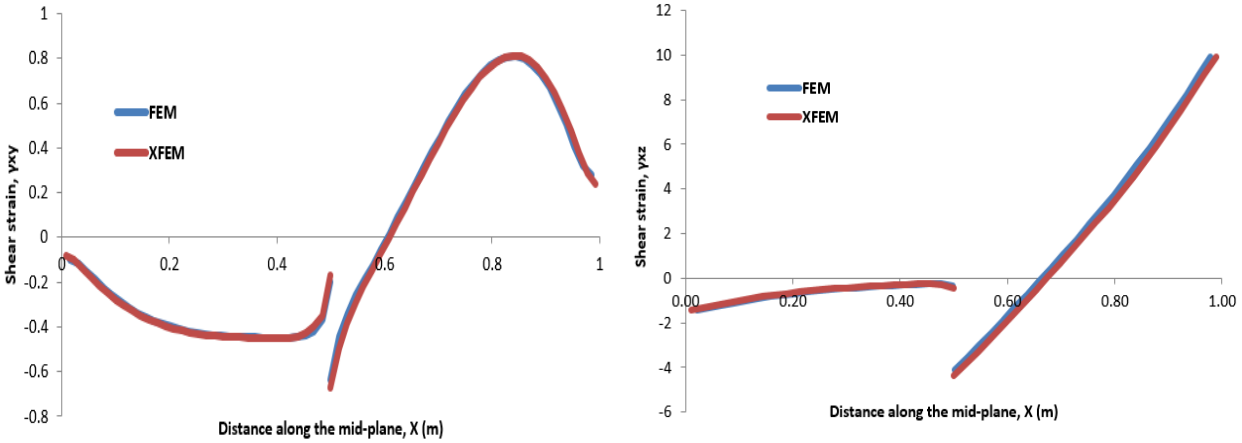


Figure 20. Comparison of shear strains γ_{xy} (left) and γ_{xz} (right) of proposed XFEM vs. FEM/ABAQUS using reduced integration technique

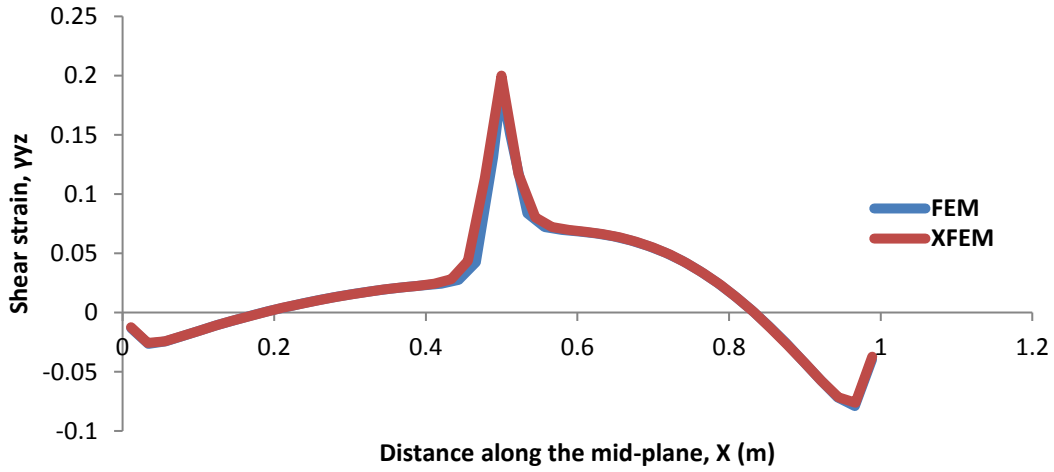


Figure 21. Comparison of shear strain in γ_{yz} of proposed XFEM vs. FEM/ABAQUS using reduced integration technique

The results show that our proposed XFEM, (where the displacement field and the shear strain fields, γ_{xz} and γ_{yz} are enriched) introduced in section 3, is in good correlation with the traditional FEM/ABAQUS.

7.3.2. Fully-clamped circular plate under concentrated force

As another example, a circular clamped plate subjected to a concentrated load P at the plate centroid is analysed (Figure 22). The interface is considered to propagate with a constant radial velocity, $\dot{r}(t) = A$ with, $r(0) = 0$ and $r(t_f) = \mathrm{R}$ $(0 \le t \le t_f)$. The modulus of elasticity and Poisson ratio are thus functions of radius at every instant of time. This implies,

$$r(t) = \frac{R}{t_f} t \ , \ E(r) = \begin{cases} E_1 \ when \ r(t) < r < R \\ E_2 \ when \ 0 < r < r(t) \end{cases}, \quad \nu(r) = \begin{cases} \nu_1 \ when \ r(t) < r < R \\ \nu_2 \ when \ 0 < r < r(t) \end{cases} \tag{30}$$

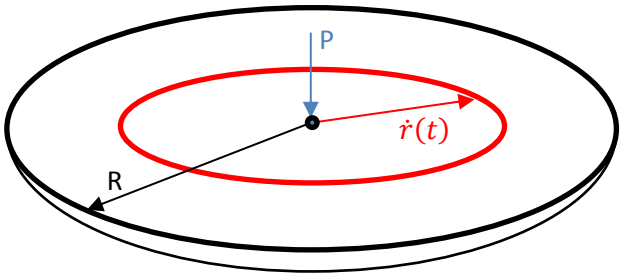


Figure 22. Clamped circular plate with thickness, t and radius R, subjected to a concentrated load P at the plate's centroid. The interface propagates with a constant radial speed of $\dot{r}(t) = A$

where in equation (30), $r(t)$ is the distance from the discontinuity front measured from the plate centre at time t and r is the distance of the point at which to obtain deflection measured from the centre. The results (deflection at the centroid of the circle) from the proposed XFEM have been compared to a combination of analytical and numerical solutions (using a very fine mesh). It can be noticed that at times $t = 0$ and $t = t_f$ the plate is homogeneous and as a result the analytical deflection for a homogeneous clamped circular plate subjected to concentrated force at the centre is given by [28], as follows:

$$w(r) = \frac{PR^2}{16\pi D}\left[1 - \left(\frac{r}{R}\right)^2 + 2\left(\frac{r}{R}\right)^2 \ln\left(\frac{r}{R}\right)\right] \tag{31}$$

Where

$$D = \frac{Et^3}{12(1-\nu^2)} \tag{32}$$

Note that the analytical solution of a Mindlin–Reissner plate (in equation (31)), exhibits a singularity at the location of the point load, thus for comparison in the vicinity of the point of singularity the analytical solution is evaluated at $r = 10^{-4}R$. Furthermore, when $0 < t < t_f$, i.e. $0 < r(t) < R$, there is no analytical solution in the literature as a result numerical solutions using ABAQUS with fine mesh have been used to extract the solution as accurately as possible.

The material properties, applied load and the dimensions of the circular plate are taken as follows:

$$P = 1\ (N), \mathrm{R} = 10\ (m), \mathrm{t} = 0.02, E_1 = 3\ (MPa), \nu_1 = 0.3, E_2 = 1\ (MPa), \nu_2 = 0.25$$

Figure 23 illustrates the results for the deflection at the centre of the plate as the interface propagates. The results obtained from the proposed XFEM correlate very well with the analytical and the numerical solutions (using a very fine mesh in ABAQUS).

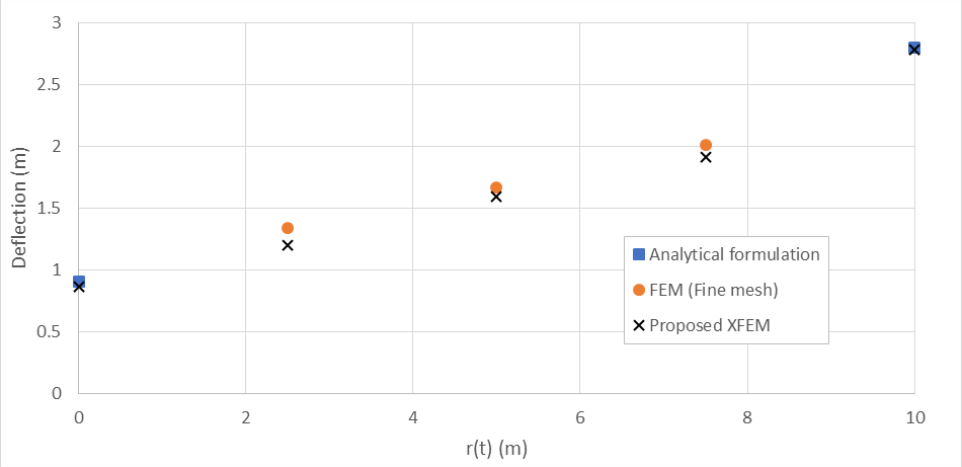


Figure 23. Comparison between the results obtained from the proposed XFEM formulation and the analytical and numerical solutions extracted from ABAQUS

It is important to mention that in the case of interface propagation, XFEM has a major advantage over FEM, as in the latter case, the element edges need to coincide with the interface of the discontinuity which requires remeshing as the interface propagates. As a result, employing FEM when dealing with moving interfaces can be computationally costly, whereas when adopting XFEM, the discontinuity can propagate through elements. This has been demonstrated in Figure 24.

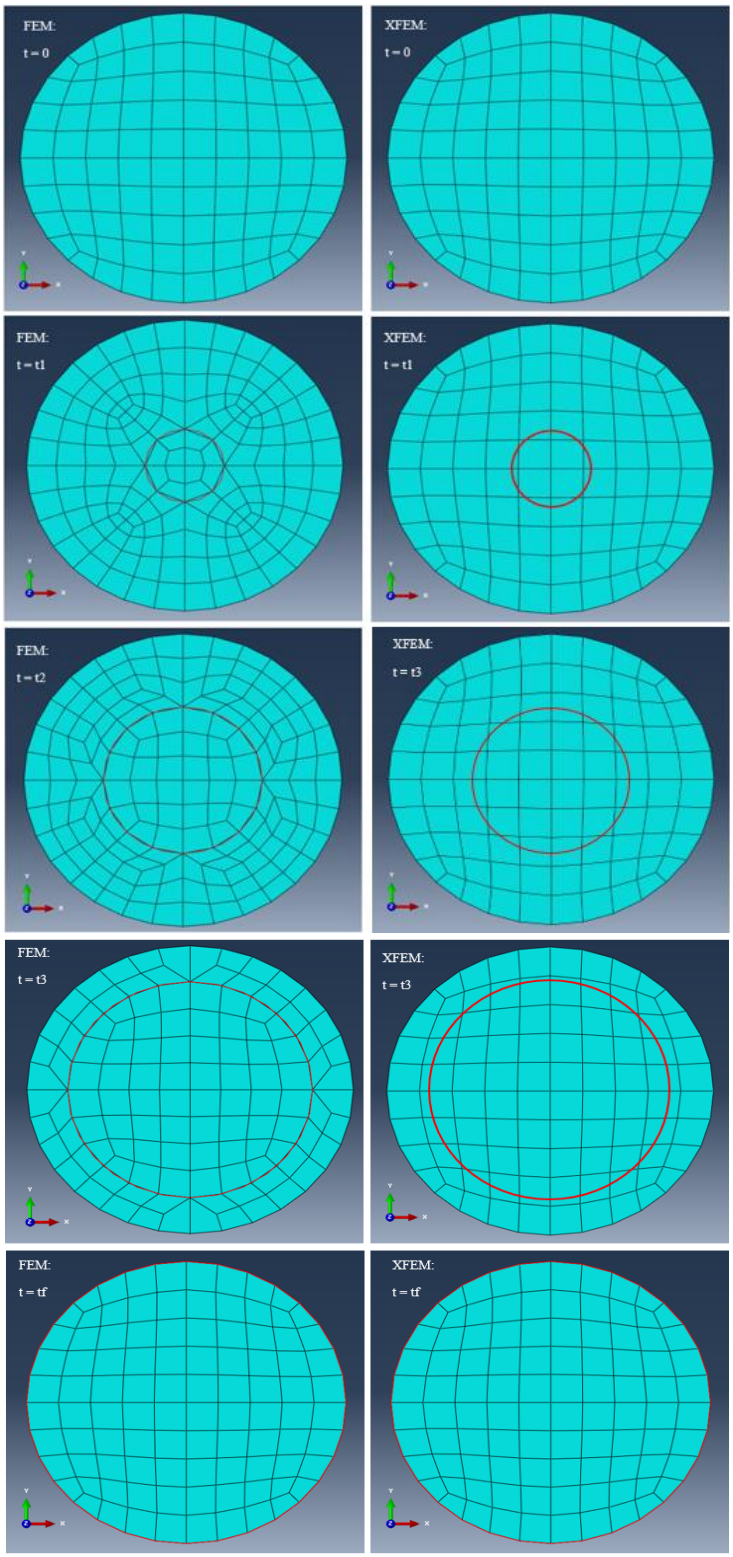


Figure 24. Comparison of FEM and XFEM meshes at different times. Remeshing is required at each time step when FEM is adopted whereas in the case of XFEM the mesh is fixed.

7.3.3. Fully-clamped rectangular plate with sweeping discontinuity front

A clamped rectangular (square) plate subjected to a central point load is analysed as shown in Figure 25. The interface is a line ($y = f(x)$) passing through a fixed point (the corner of the plate) and is considered to propagate with a constant angular velocity, $\dot{\theta}(t) = k$ with, $\theta(0) = 0$ and $\theta(t_f) = \pi/2$ $(0 \le t \le t_f)$ and sweeping the entire plate. This implies:

$$y(x,t) = tan\left(\frac{\pi t}{2t_f}\right)x\,,\ E(x,y) = \begin{cases} E_1\ when\ y > f(x) \\ E_2\ when\ y < f(x) \end{cases}\,,\ \nu(x,y) = \begin{cases} \nu_1\ when\ y > f(x) \\ \nu_2\ when\ y < f(x) \end{cases} \qquad (33)$$

As in the previous example, the results (deflection at the centre of the plate) from the proposed XFEM have been compared to a combination of analytical and numerical solutions (FEM/ABAQUS using a very fine mesh).

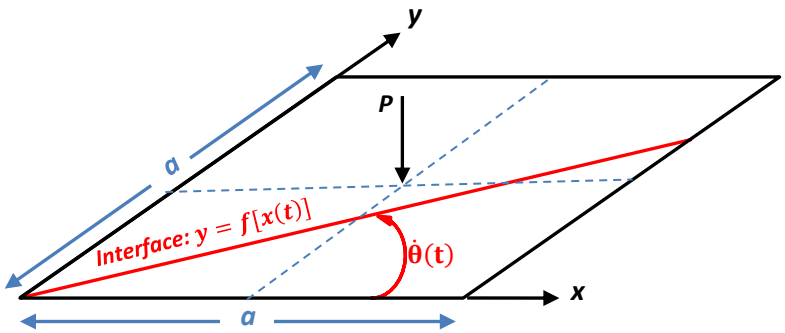


Figure 25. Clamped square plate with thickness, t and side length a, subjected to a concentrated load P at the plate's centre. The interface propagates with a constant angular speed of, $\dot{\theta}(t) = k$

The material properties, applied load and the dimensions of the square plate are as follows:

$$P = 100\ (N), a = 80\ (m), \mathrm{t} = 0.8, E_1 = 3\ (MPa), \nu_1 = 0.3, E_2 = 1\ (MPa), \nu_2 = 0.3$$

Once more, it is noticed that at times $t = 0$ and $t = t_f$ the plate is homogeneous as a result of which the analytical solution for this problem can be found in the literature [28], where the deflection at the plate centroid is:

$$w_o = \mathrm{c}\frac{Pa^2}{D} \qquad (34)$$

where the coefficient c is a function of the dimension ratio, a (see [28]) and D is the flexural rigidity of plate as defined by equation (32).

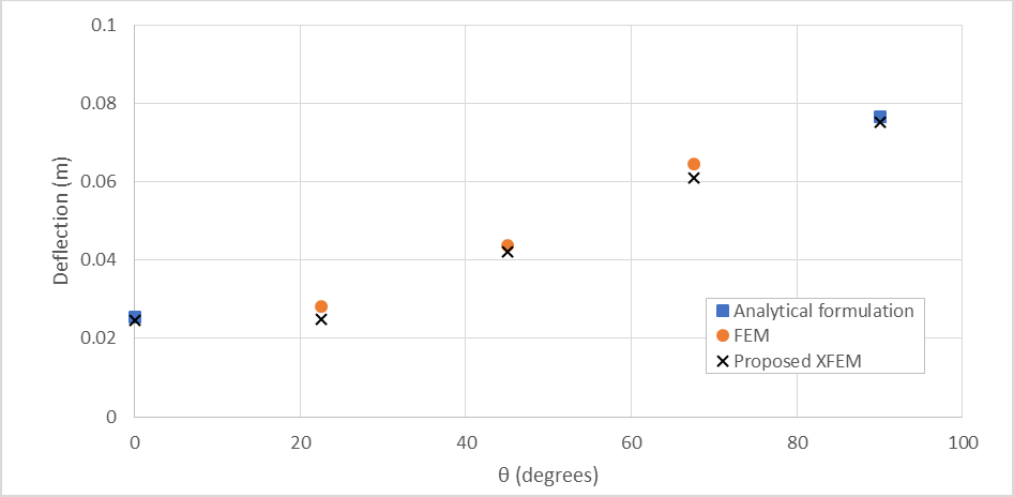


Figure 26. Comparison of midpoint deflection between the results obtained from the proposed XFEM formulation and the analytical, and other numerical solutions extracted from ABAQUS for a square plate with radially propagating discontinuous front

Moreover, when $0 < t < t_f$, the numerical solution using ABAQUS with a fine mesh has been used to evaluate the response as accurately as possible. Figure 26 illustrate the results of the deflection at the centre of the plate as the interface propagates. The results obtained from the proposed XFEM correlate very well with both the analytical and numerical solutions (using a very fine mesh in ABAQUS). Again, as in the previous example, the advantage of adopting XFEM over FEM when dealing with moving interfaces has been demonstrated in Figure 27.

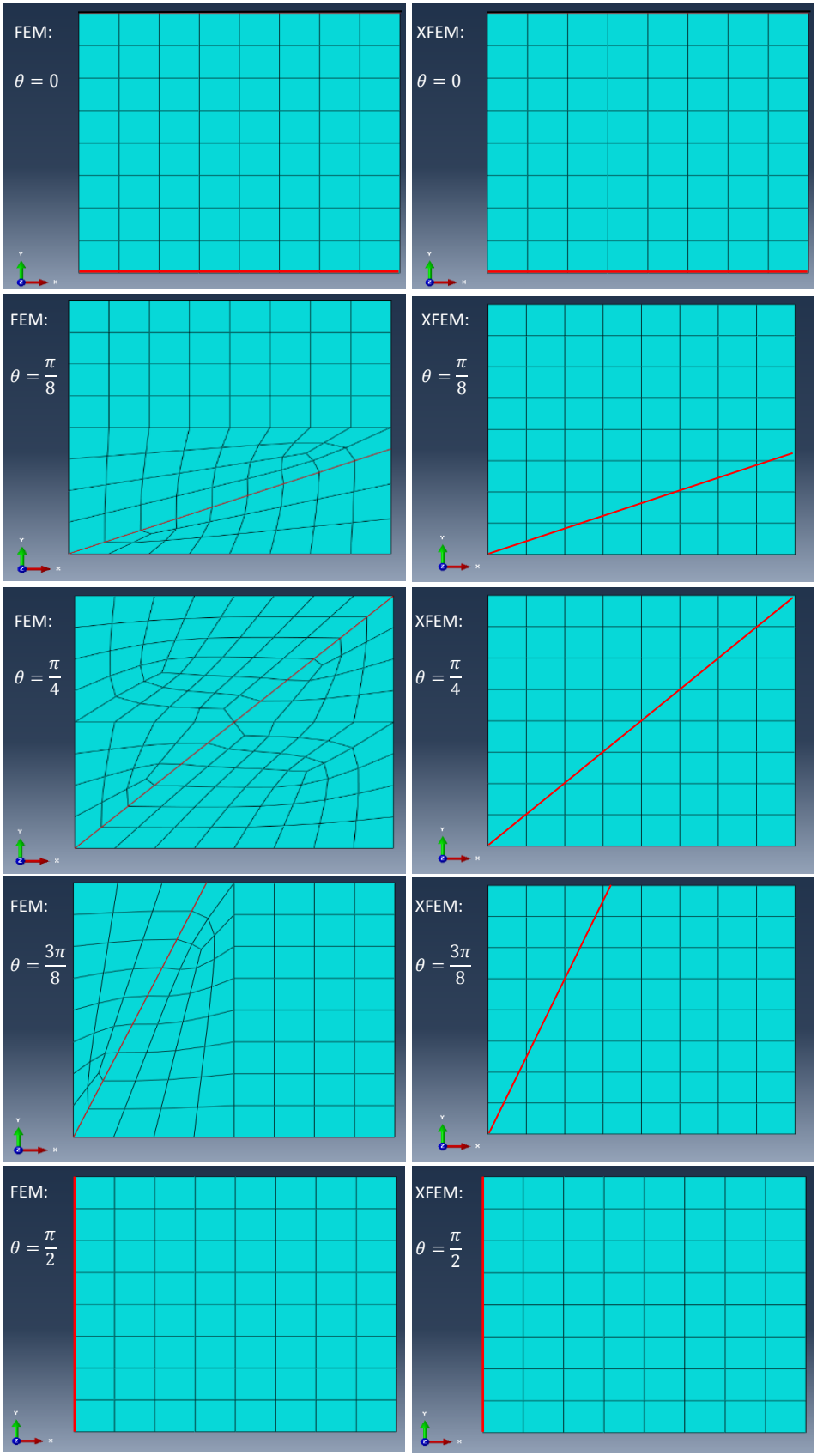


Figure 27. Comparison between FEM and XFEM meshes for the square plate under consideration at different times. Remeshing is required at each time step when FEM is adopted whereas in the case of XFEM the mesh is fixed.

8. Conclusions

In this paper the authors have introduced enhanced MITC Timoshenko beam and Mindlin-Reissner plate elements in conjunction with XFEM that do not lock. In the subsequent sections the conclusions drawn based on the analyses conducted in this paper are discussed separately.

A new shear locking-free mixed interpolation Timoshenko beam element was used to study weak discontinuity in beams. Weak discontinuity in beams of all depth-to-length ratio may emerge as a result of certain functionality requirement (as in a thermostat), or as a consequence of a particular phenomenon (as oxidisation). The formulation was based on the Hellinger-Reissner (HR) functional applied to a Timoshenko beam with displacement and out-of-plane shear strain degrees-of-freedom (which were later reduced to the displacement as the degree-of-freedom). The proposed locking-free XFEM formulation is novel in its aspect of adopting enrichment in strain as a degree-of-freedom allowing to capture a jump discontinuity in strain. The formulation avoids shear locking for monolithic beams and the results were shown promising. In this study heterogeneous beams were considered and the mixed formulation was combined with XFEM thus mixed enrichment functions have been adopted. The enrichment type is restricted to extrinsic mesh-based topological local enrichment. The method was used to analyse a bi-material beam in conjunction with mixed formulation-mixed interpolation of tensorial components Timoshenko beam element (MITC). The bi-material was analysed under different loadings and with different elements (linear and quadratic) for the static loading case. The displacement fields and strain fields results of the proposed XFEM have been compared with the classical FEM and conventional XFEM (where only the displacement field, and not the strain field, is enriched). The results show that the proposed XFEM converges faster to the analytical solution than the other two methods and it is in good correlation with the analytical solution and those of the FEM. The proposed XFEM method captures the jump in shear strain across the discontinuity with much higher accuracy than the standard XFEM. As Figures 10-13 suggest the proposed XFEM with mixed enrichment functions (Heaviside and ramp functions) has a better convergence rate for both linear and quadratic elements compared to the standard FEM.

Further examination of the robustness of the proposed method for static problems has been undertaken and results compared with the analytical solution and standard FEM which show the accuracy of the proposed method. In the standard XFEM one only enriches the displacement field and not the shear strain but in the proposed XFEM both the displacement degrees of freedom and the shear strain degrees of freedom have been enriched. As a result of this, two different enrichment functions have been used. For the displacement field the new ramp function that has been proposed by Moës et. al. [27], and has a better rate of the convergence than the traditional ramp function specially for blending elements, has been used and for the shear strain the Heaviside step enrichment function (this has been shown and discussed in section 3) has been used. As a result of introducing the mixed enrichment function in our proposed XFEM, the shear strain and its jump across the discontinuity have been captured with much higher accuracy when compared with the traditional XFEM where

only the displacement field has been enriched. This has been shown in Figures 10-13 where the L_2-norms are compared.

The authors have further extended the proposed XFEM method from the Timoshenko beam formulation to the Mindlin-Reissner plate formulation to study weak discontinuity in plates. The formulation was based on the Hellinger-Reissner (HR) functional applied to a Mindlin-Reissner plate with displacements and out-of-plane shear strains degrees-of-freedom. One of the properties of such formulation is that it avoids shear locking and the results were shown promising. In this study a bi-material plate was considered and the mixed formulation was combined with XFEM thus mixed enrichment functions have been adopted. The displacement and strain field results of the proposed XFEM have been compared with the classical FEM/ABAQUS, which shows a good correlation between the two. As a result of enriching strains, two different enrichment functions have been used.

References

[1] F. Brezzi and G. Gilardi, "Chapters 1-3 in" Finite Element Handbook", H. Kardestuncer and DH Norrie," ed: McGraw-Hill Book Co., New York, 1987.

[2] F. Brezzi and M. Fortin, *Mixed and hybrid finite element methods* (Springer series in computational mathematics, no. 15). New York: Springer-Verlag, 1991, pp. ix, 350 p.

[3] J. N. Reddy, "A general non-linear third-order theory of plates with moderate thickness," *International Journal of Non-Linear Mechanics,* vol. 25, no. 6, pp. 677-686, 1990/01/01 1990.

[4] G. Y. Shi, "A new simple third-order shear deformation theory of plates," (in English), *International Journal of Solids and Structures,* vol. 44, no. 13, pp. 4399-4417, Jun 15 2007.

[5] M. C. Ray, "Zeroth-order shear deformation theory for laminated composite plates," (in English), *Journal of Applied Mechanics-Transactions of the Asme,* vol. 70, no. 3, pp. 374-380, May 2003.

[6] L. B. da Veiga, C. Lovadina, and A. Reali, "Avoiding shear locking for the Timoshenko beam problem via isogeometric collocation methods," (in English), *Computer Methods in Applied Mechanics and Engineering,* vol. 241, pp. 38-51, 2012.

[7] M. H. Verwoerd and A. W. M. Kok, "A shear locking free six-node mindlin plate bending element," *Computers & Structures,* vol. 36, no. 3, pp. 547-551, 1990/01/01 1990.

[8] K.-J. Bathe and E. N. Dvorkin, "A four-node plate bending element based on Mindlin/Reissner plate theory and a mixed interpolation," *International Journal for Numerical Methods in Engineering,* vol. 21, no. 2, pp. 367-383, 1985.

[9] N. D. Eduardo and B. Klaus-Jürgen, "A continuum mechanics based four-node shell element for general non-linear analysis," *Engineering Computations,* vol. 1, no. 1, pp. 77-88, 1984/01/01 1984.

[10] K.-J. r. Bathe and K.-J. r. Bathe, *Finite element procedures*. Englewood Cliffs, N.J.: Prentice Hall, 1996, pp. xiv, 1037 p.

[11] I. Babuska and J. M. Melenk, "The partition of unity method," (in English), *International Journal for Numerical Methods in Engineering,* vol. 40, no. 4, pp. 727-758, Feb 28 1997.

[12] J. Dolbow, N. Moes, and T. Belytschko, "Modeling fracture in Mindlin-Reissner plates with the extended finite element method," (in English), *International Journal of Solids and Structures,* vol. 37, no. 48-50, pp. 7161-7183, Nov-Dec 2000.

[13] N. Moes and T. Belytschko, "Extended finite element method for cohesive crack growth," (in English), *Engineering Fracture Mechanics,* vol. 69, no. 7, pp. 813-833, May 2002.

[14] N. Sukumar, D. L. Chopp, N. Moes, and T. Belytschko, "Modeling holes and inclusions by level sets in the extended finite-element method," (in English), *Computer Methods in Applied Mechanics and Engineering,* vol. 190, no. 46-47, pp. 6183-6200, 2001.

[15] M. Toolabi, A. S. Fallah, P. M. Baiz, and L. A. Louca, "Dynamic analysis of a viscoelastic orthotropic cracked body using the extended finite element method," (in English), *Engineering Fracture Mechanics,* vol. 109, pp. 17-32, Sep 2013.
[16] J. Xu, C. K. Lee, and K. Tan, "An XFEM plate element for high gradient zones resulted from yield lines," *International Journal for Numerical Methods in Engineering,* vol. 93, no. 12, pp. 1314-1344, 2013.
[17] N. Moes, J. Dolbow, and T. Belytschko, "A finite element method for crack growth without remeshing," (in English), *International Journal for Numerical Methods in Engineering,* vol. 46, no. 1, pp. 131-150, Sep 10 1999.
[18] S. Natarajan, S. Chakraborty, M. Ganapathi, and M. Subramanian, "A parametric study on the buckling of functionally graded material plates with internal discontinuities using the partition of unity method," *European Journal of Mechanics A/Solids,* vol. 44, pp. 136-147, 2014.
[19] F. van der Meer, "A level set model for delamination in composite materials," *Numerical Modelling of Failure in Advanced Composite Materials,* p. 93, 2015.
[20] S. Peng, "Fracture of Shells with Continuum-Based Shell Elements by Phantom Node Version of XFEM," Northwestern University, 2013.
[21] P. Baiz, S. Natarajan, S. Bordas, P. Kerfriden, and T. Rabczuk, "Linear buckling analysis of cracked plates by SFEM and XFEM," *Journal of Mechanics of Materials and Structures,* vol. 6, no. 9, pp. 1213-1238, 2012.
[22] R. Larsson, J. Mediavilla, and M. Fagerström, "Dynamic fracture modeling in shell structures based on XFEM," *International Journal for Numerical Methods in Engineering,* vol. 86, no. 4-5, pp. 499-527, 2011.
[23] A. Moysidis and V. Koumousis, "Hysteretic plate finite element," *Journal of Engineering Mechanics,* vol. 141, no. 10, p. 04015039, 2015.
[24] H.-M. Jeon, P.-S. Lee, and K.-J. Bathe, "The MITC3 shell finite element enriched by interpolation covers," *Computers & Structures,* vol. 134, pp. 128-142, 2014.
[25] Y. Ko, P.-S. Lee, and K.-J. Bathe, "A new 4-node MITC element for analysis of two-dimensional solids and its formulation in a shell element," *Computers & Structures,* vol. 192, pp. 34-49, 2017.
[26] J. Xu, C. K. Lee, and K. H. Tan, "An enriched 6-node MITC plate element for yield line analysis," in *Computers & Structures*, 2013, vol. 128, pp. 64-76.
[27] N. Moes, M. Cloirec, P. Cartraud, and J. F. Remacle, "A computational approach to handle complex microstructure geometries," (in English), *Computer Methods in Applied Mechanics and Engineering,* vol. 192, no. 28-30, pp. 3163-3177, 2003.
[28] S. P. Timoshenko and S. Woinowsky-Krieger, *Theory of plates and shells*. McGraw-hill, 1959.

Appendix A

The governing equations for a beam under pressure which consists of two different materials (Figure 3a) with respect to the Timoshenko beam theory are,

$$\frac{\partial}{\partial x}\left[E(x)I\frac{\partial\theta}{\partial x}\right]+\kappa AG(x)\left[\frac{\partial w}{\partial x}-\theta\right]=0 \qquad (A1)$$

$$\frac{\partial}{\partial x}\left[\kappa AG(x)\left(\frac{\partial w}{\partial x}-\theta\right)\right]+q(x)=0 \qquad (A2)$$

where θ is the section rotation, w is the vertical displacement, E is the Young's modulus, G is the Shear modulus, κ is the shear correction factor, I is the second moment of area, q is the shear force and A is the section area.

Rearranging (A1) and substituting it into (A2),

$$\frac{\partial^2}{\partial x^2}\left[E(x)I\frac{\partial\theta}{\partial x}\right]=q(x) \qquad (A3)$$

Integrating (A3) twice with respect to x,

$$\frac{\partial\theta}{\partial x}=\frac{\int(\int q(x)\,dx)\,dx}{E(x)I} \qquad (A4)$$

Where,

$$E(x)=\begin{cases}E1 & x<x^*\\ E2 & x\geq x^*\end{cases}, \quad x^* \text{ is the position of material interface} \qquad (A5)$$

Integrating (A4) with respect to x,

$$\theta(x)=\int\frac{\int(\int q(x)\,dx)\,dx}{E(x)I}dx \qquad (A6)$$

Substituting (A6) into (A1) and rearranging,

$$\frac{\partial w}{\partial x}=\theta-\frac{\frac{\partial}{\partial x}\left[E(x)I\frac{\partial\theta}{\partial x}\right]}{\kappa AG(x)} \qquad (A7)$$

Now integrating (A7) with respect to x,

$$w(x)=\int\left[\theta-\frac{\frac{\partial}{\partial x}\left[E(x)I\frac{\partial\theta}{\partial x}\right]}{\kappa AG(x)}\right]dx \qquad (A8)$$

Where,

$$G(x) = \begin{cases} G1 & x < x^* \\ G2 & x \geq x^* \end{cases}, \qquad x^* \; is \; the \; position \; of \; material \; interface \qquad (A9)$$

In this paper the examples that are considered are as follow,

1) Cantilever beam under uniformly distributed load (i.e. $q(x) = constant$)
2) Cantilever beam under linear loading (i.e. $q(x) = ax + b$)

And the boundary conditions and continuity equations are as follow due to the chosen cantilever beam example,

(1) $w_1(0) = 0$
(2) $\theta_1(0) = 0$
(3) $M_2(L) = E_2 I \frac{\partial \theta_2}{\partial x}\Big|_{x=L} = 0$
(4) $Q_{2_{xz}}(L) = \kappa A G_2 \left(\frac{\partial w_2}{\partial x} - \theta_2\right)\Big|_{x=L} = 0$
(5) $\theta_1(x^*) = \theta_2(x^*)$
(6) $w_1(x^*) = w_2(x^*)$
(7) $M_1(x^*) = M_2(x^*)$
(8) $Q_{1_{xz}}(x^*) = Q_{2_{xz}}(x^*)$

where subscribe 1 denotes the variables related to the section with material 1 property and subscribe 2 are the variables related to the section with the second material property.

Below, is the solution (displacements and through thickness shear strains of beams 1 and 2) when the loading in case 1 (Cantilever beam under uniformly distributed load i.e. $q(x) = constant$) is applied,

$$\theta_1(x) = \frac{q}{6E_1 I}x^3 - \frac{qL}{2E_1 I}x^2 + \frac{qL^2}{2E_1 I}x \qquad (A10)$$

$$\theta_2(x) = \theta_1(x^*) + (x - x^*)f(x) \qquad (A11)$$

$$w_1(x) = \frac{q}{24E_1 I}x^4 - \frac{qL}{6E_1 I}x^3 + \left(\frac{qL^2}{4E_1 I} - \frac{q}{2\kappa A G_1}\right)x^2 + \frac{qL}{\kappa A G_1}x \qquad (A12)$$

$$w_2(x) = w_1(x^*) + (x - x^*)f(x) \qquad (A13)$$

$$\gamma_{1_{xz}}(x) = \frac{-q}{\kappa A G_1}x + \frac{qL}{\kappa A G_1} \qquad (A14)$$

$$\gamma_{2_{xz}}(x) = \frac{-q}{\kappa A G_2}x + \frac{qL}{\kappa A G_2} \qquad (A15)$$

Where x is the distance from the boundary, x^* is the position of the material discontinuity and $\gamma_{i_{xz}}\ i = 1,2$ is the through thickness shear strain. The same procedures can be followed in the case of UDL.